Failure behavior of the surrounding rock of jointed rock masses in a gold mine under impact disturbance

Peng Li
University of Science and Technology Beijing
Yunquan Wu (wu_yunquan@163.com)
University of Science and Technology Beijing
Meifeng Cai
University of Science and Technology Beijing

Research Article

Keywords: Jointed rock mass; Impact disturbance; Discrete element method, Failure mechanism, Influence factor

Posted Date: February 25th, 2021

DOI: https://doi.org/10.21203/rs.3.rs-236125/v1

Failure behavior of the surrounding rock of jointed rock masses in a gold mine under impact disturbance

Peng Li[1,2,3] · Yun-quan Wu[1,2,3] · Mei-feng Cai[1,2,3]

✉ Yun-quan Wu
wu_yunquan@163.com

[1] School of Civil and Resource Engineering, University of Science and Technology Beijing, Beijing 100083, China

[2] Key Laboratory of High-Efficient Mining and Safety of Metal Mines (Ministry of Education of China), University of Science and Technology Beijing, Beijing 100083, China

[3] Beijing Key Laboratory of Urban Underground Space Engineering, University of Science and Technology Beijing, Beijing 100083, China

Abstract: The impact disturbance has an important influence on the safety of underground engineering openings. In this paper, based on the in-situ stress measurement and structural plane investigation, the model of jointed rock roadway was established using the discrete element method (3DEC) to study the instability and failure characteristic of roadway surrounding rock with dominant joint planes under impact disturbance and to further analyze the influence of different buried depths, impact stress wave peaks, and stress wave delays on the stability of the surrounding rock. The results show that the stability of the surrounding rock is poor, and the whole convergence deformation of the surrounding rock occurs under the impact stress wave. There are three failure modes in the surrounding rock: tensile-shear failure, tensile failure, and shear failure. Tensile-shear failure mainly occurs in a small range close to the roof and floor of the roadway and the free surfaces of the two sides, and tensile failure occurs locally, while shear failure mainly occurs along the joint plane outside this range. Moreover, the greater the buried depth and stress wave peak value, the more serious the deformation of the surrounding rock. With the increase of stress wave delay, the deformation of the surrounding rock shows complex characteristics. In addition, the impact failure mechanism of the surrounding rock in jointed rock masses was discussed. The research results have important guiding significance for the prevention and control of underground engineering cavern disasters.

Keywords: Jointed rock mass; Impact disturbance; Discrete element method; Failure mechanism; Influence factor

Introduction

The safety of surrounding rock in underground engineering has always been an important research direction in mining engineering (Li et al. 2019b). As we know, a series of supporting tunnels and shafts will be built in underground mines before mining, which are important channels to ensure the normal production and safe operation of the mines. During construction or service, the surrounding rock of the roadway may not be destroyed when the internal stress reaches the destruction strength and maybe in a subcritical or critical equilibrium state. However, when it is strongly disturbed by external dynamics (such as blasting vibration, rock burst, and seismic activity), the surrounding rock of the roadway may be unstable and destroyed. In particular, the stability of the roadway surrounding rock with developed joints and fissures is poor, which is more likely to cause instability and failure after being disturbed by the external force.

To investigate the influence of dynamic disturbance on the underground cavity in practical engineering, some scholars have studied the instability and failure behavior of surrounding rock of chamber under impact dynamic load. Pan et al. (2011) studied the dynamic failure process of the roadway under high-speed impact load using explosion loading similar simulation test and digital speckle observation method. Deng et al. (2014) simulated the damage of the existing circular tunnel under the action of explosion shock wave based on the discrete element software UDEC and pointed out that the direction of joints in the rock mass around the tunnel has a great influence on the tunnel damage. Li et al. (2015) believed that under the impact load, marble samples with chambers would produce initial tensile cracks and X-like initial shear cracks parallel to the axial loading direction around the chambers, which played a leading role in the failure of the samples. Li et al. (2016) studied the fracture process of porous sandstone samples under

static and dynamic combined loading and suggested that under the action of dynamic load, the location of surface crack initiation will be randomly distributed, and the specimen will eventually form pits with circular openings. Tao et al. (2017) stated that the combined action of high static prestresses and dynamic load promotes rock debris to eject to the surrounding round hole, and the combined action of static stress concentration and dynamic stress concentration induced the primary fracture of rock. Han et al. (2018) found that macro-scale cracks mostly start at or near the tip of the elliptical chamber, and then propagate in different paths with different crack geometries. Weng et al. (2018) observed that prestress and subsequent dynamic load cause circumferential stress concentration around the chamber, and the fracture of the specimen starts from the maximum circumferential stress concentration area. Previous studies have contributed to revealing the instability and failure mechanism of the surrounding rock of the chamber. However, the problem of dynamic stability of surrounding rock of cavern under dynamic impact disturbance mainly focuses on the laboratory scale, and the research on dynamic stability of surrounding rock of jointed rock roadway under dynamic impact disturbance under certain buried depth is very scarce. In addition, with the development and wide application of numerical simulation technology, a large number of numerical simulation software are used in engineering research, which can make up for some defects that can not be realized in laboratory experiments.

For this purpose, in the present study, a typical roadway at the depth of 915 m in a gold mine in Shandong Province of China is taken as the concrete engineering background. Based on the determined dominant occurrence of the structural plane in the surrounding rock of the roadway and the in-situ stress measurement results, the corresponding numerical model of jointed rock roadway is established using the 3DEC software, and the stability of the surrounding rock of the roadway with dominant joint planes under impact disturbance. Subsequently, the characteristics of surrounding rock deformation and failure of jointed rock roadway under different buried depths, impact stress wave peaks, and impact stress wave delays are further analyzed. On this basis, the impact failure mechanism of the surrounding rock of jointed rock roadway is discussed to provide guidance for prevention and control of engineering dynamic disasters.

Engineering background

A gold mine is geographically located in Jiaodong Peninsula, Shandong Province, China (Fig. 1). It is one of the largest underground metal mines in China, and its mining depth exceeds 1000 m underground at present. The gold deposits in the mining area belong to a super-large structural altered rock type gold deposit, in which the rock alteration is serious, the surrounding rock is broken, and the structural weak planes are crisscrossed. With the increase of mining depth, the engineering geological conditions become more and more complex, and the joints and fissures in deep rock masses are relatively developed. Besides, under the high in-situ stress condition, the mine ground pressure behavior is becoming more and more prominent, and the frequency and intensity of disasters such as large deformation, spalling, roof fall, and the collapse of surrounding rock of the roadway are on the rise and have a strong tendency of impact, which greatly weakens the stability of the roadway, seriously threatens the safety of workers, and affects the normal production of mine.

The roadway surrounding rock at the depth of 915 m in the gold mine is mainly sericitolited granite, showing obvious redundant granite structure and massive structure, with well-developed joints and fissures, belonging to Class III or IV surrounding rock. The roadway is not only subjected to high in-situ stress but also affected by mining disturbances such as frequent blasting operations in adjacent stopes. The surrounding rock of the roadway appears spalling and local roof fall, and the deformation and damage problems are serious. The typical deformation of surrounding rock in local areas is shown in Fig. 1. The stability of the surrounding rock of the jointed rock roadway is a thorny problem in the deep mining of mineral resources in this mine. The development of joints and other structural planes greatly weakens the overall stability of the roadway surrounding rock and often becomes the key factor of roadway instability and failure. Moreover, the existence of structural planes will cause geological uneven ground pressure in the surrounding rock of the jointed rock roadway, resulting in the complicated and changeable failure modes of the roadway. Consequently, it is particularly necessary to investigate the instability and failure mechanism of the surrounding rock of the jointed rock roadway in the mine.

Fig. 1

In-situ stress measurement and structural plane investigation in the mine

In-situ stress measurement

In-situ stress is the fundamental driving force leading to instability and failure of the surrounding rock of openings in underground engineering. Numerous studies show that the stability of underground openings such as roadways and shafts and the engineering dynamic disasters characterized by rock burst that may occur during mining are directly related to the in-situ stress environment in the engineering area (Li et al. 2018).

To ascertain the in-situ stress state of the gold mine area and then provide the basis for the construction of deep roadways and the optimization design of supporting structures, the overcoring method with an improved CSIRO hollow inclusion stress gauge (Fig. 2) was adopted to determine the in-situ stress conditions in the mining area for multiple periods. This method that suggested by the International Society for Rock Mechanics (ISRM) (Li et al. 2019a) is a highly maturing technique for characterizing the real stress state including both magnitude and orientation with the advantages of high measurement accuracy, simple installation and operation, and low cost. A large number of in-situ stress data at different levels in the mine were obtained. The in-situ stress measurement results are presented in Table 1. The principle and method of using the improved CSIRO to measure the in-situ stress can be found in the introduction of Cai et al. (2002). Note that some new technologies such as complete temperature compensation technology and automatic data acquisition and recording system were applied in the measurement process, which greatly improved the reliability and accuracy of in-situ stress measurement results.

Fig. 2

Table 1

According to the measured in-situ stress data shown in Table 1, it is found that two of the three principal stresses are located in the near horizontal direction, and the absolute values of dip angles are less than 20°. The other principal stress is close to the vertical direction, and the absolute values of dip angles are all greater than 70°. In addition, the in-situ stress distribution law (in-situ stress field model) of the mining area can be obtained as follows:

$$\sigma_H = 0.0401H + 3.1806 \quad (R^2 = 0.9682) \tag{1}$$

$$\sigma_h = 0.0245H + 1.4234 \quad (R^2 = 0.8137) \tag{2}$$

$$\sigma_h = 0.0259H + 0.8276 \quad (R^2 = 0.9443) \tag{3}$$

where σ_H, σ_h, and σ_v are the maximum horizontal, minimum horizontal, and vertical principal stress, respectively; H is the buried depth; R is the correlation coefficient.

It can be seen from Eqs. (1)–(3) that the correlation coefficient values are very high, and the in-situ stress magnitudes of the mine increase linearly with depth. According to the linear fitting equation, the calculated σ_H, σ_h, and σ_v at the depth of 915 m are approximately 39.87 MPa, 24.53 MPa, and 23.84 MPa, respectively, which can provide a more realistic stress boundary condition for later engineering numerical simulation calculation.

Structural plane investigation

Due to the well-developed joints and fissures in this mining area, it is very important to investigate the distribution of structural planes in order to analyze the stability of roadway surrounding rock in jointed rock mass in this mining area. ShapeMetrix 3D digital photogrammetry system (Fig. 3a) is usually employed in the structural plane investigation. The measuring principle of the system is to import the left and right views obtained from the site into ShapeMetrix 3D software analysis system (Fig. 3b), and delineate the key measuring areas. According to a series of technologies such as pixel matching and image deformation deviation correction, the system synthesizes the three-dimensional model and realizes the orientation and distance, thus obtaining the three-dimensional view of the rock mass surface. The system can quickly, accurately, and quantitatively obtain the geometric shape and attitude characteristic parameters of the structural plane of the surrounding rock mass in the engineering field using non-contact measurement, which greatly reduces the manual workload and human error, and can accurately and reliably determine the field data.

Fig. 3

In this paper, the ShapeMetrix 3D digital photogrammetry system was used to collect digital images of surrounding rock of the roadway at the depth of 915 m in the mining area, and the images were imported into the matching software analysis system to process the images, and a three-dimensional reconstruction model of surrounding rock surface of the roadway can be obtained. The dimension and orientation of the model were realized, the geometric information of the joints and fissures of the surrounding rock was determined, and the three-dimensional visualization model of the jointed rock mass was obtained. Moreover, the data of trace length, inclination, dip angle, and spacing of the identified structural planes were analyzed by mathematical statistics. Subsequently, the stereographic projection diagram of the structural planes was drawn by stereographic projection analysis and cluster analysis, and finally, the dominant structural plane occurrence was obtained by statistics, which can provide structural plane information for numerical simulation analysis of the stability of the surrounding rock of the roadway. The information collection and processing process of the structural plane of the surrounding rock of the roadway are shown in Fig. 4.

According to the stereographic projection, two groups of dominant structural planes of the roadway were determined. The dominant occurrences of the two groups are 234.24°∠51.04° and 327.47°∠53.89°, respectively, and the average joint spacings of the two groups are approximately 0.4 m and 0.3 m, respectively.

Fig. 4

Failure behavior of the surrounding rock of jointed rock roadway under impact disturbance

Establishment of the numerical model of jointed rock roadway

Principle of discrete element numerical calculation

3 Dimensional Distinct Element Code (3DEC) is a three-dimensional discrete element method program developed by ITASCA company in the United States to deal with discontinuous media, which can be used to simulate the mechanical response behavior of discontinuous media under static or dynamic loads. More importantly, the 3DEC allows large displacement and rotation of blocks in the model along discontinuous surfaces and is an effective tool to study the potential failure characteristics of discontinuous media (Israelsson 1996), which has been widely used in the analysis of chamber surrounding rock stability and slope stability in mining engineering.

The basic solution equations in 3DEC are mainly physical and motion equations, of which dynamic calculation is based on Newton's second law:

$$d\dot{u}/dt = F/m \tag{4}$$

The central difference method was adopted to solve Eq. (4), which can be transformed into the following:

$$d\dot{u}/dt = [\dot{u}(t+\Delta t/2) - \dot{u}(t-\Delta t/2)]/\Delta t \tag{5}$$

Further,

$$\dot{u}_i(t+\Delta t/2) = \dot{u}_i(t-\Delta t/2) + [(\sum F_i(t))/\mathrm{m} + g_i]\Delta t \tag{6}$$

$$\dot{v}_i(t+\Delta t/2) = \dot{v}_i(t-\Delta t/2) + [(\sum N(t))/M]\Delta t \tag{7}$$

After considering damping, the basic dynamic equation can be expressed as follows:

$$m\ddot{u}(t) + \mathrm{c}\dot{u}(t) + ku(t) = f(t) \tag{8}$$

where u is the unit displacement; T is time; C is damping coefficient; F is the external load; K is the elastic stiffness coefficient; M is the mass.

The central difference method in the 3DEC software is used for the dynamic solution. This method is an explicit algorithm in which a suitable damping coefficient needs to be determined.

Model building

The cross-section of the roadway at the depth of 915 m in the mine is in the form of a straight wall arch, with the size of 4.2 m × 3.4 m (width × height) and arch height of 1.05 m, as shown in Fig. 5a. In this study, the 3DEC software was used to establish the numerical calculation model. In the 3DEC model, the more blocks and contact surfaces, the longer the calculation time. At the same time, considering the propagation of the stress wave and the existing hardware conditions, it is necessary to determine the appropriate model size. After several attempts, the model size was determined to be 30 m × 10 m× 30 m (length × width × height), and the roadway size in the model is consistent with its actual size. The calculation model after the excavation is illustrated in Fig. 5b.

Fig. 5

According to the two groups of dominant structural planes identified above, two groups of through joints were added to the model. The first group of joints inclines 234.24° and an included angle with the horizontal plane of 51.04°; the inclination of the second joint group is 327.47°, and the included angle with the horizontal plane is 53.89°. To improve the efficiency of dynamic operation and save memory, the added joints were simplified appropriately, that is, the distance between each group of dominant joint planes in the model was expanded to twice the actual statistical distance, which was 0.8 m and 0.6 m, respectively. In addition, all joints were treated as plane joints without considering the roughness of the joints.

The model in 3DEC is usually composed of tetrahedral elements. Theoretically, the smaller the mesh size, the higher the calculation accuracy. This, however, will greatly reduce the calculation speed and even cause unexpected failures in the calculation. Lysmer and Kuhlemeyer (1969) believed that the wave propagation can be well simulated when the grid size Δl was less than 1/8–1/10 of the wavelength corresponding to the highest frequency of the input waveform, i.e.,

$$\Delta l \leq \lambda/10 \sim \lambda/8 \tag{9}$$

$$\lambda = c/f \tag{10}$$

where Δl is the maximum length of triangular mesh element along the wave propagation direction; λ is the maximum wavelength; f is the wave frequency; c is the wave propagation velocity.

The tetrahedron element formula in the 3DEC model is non-equilateral, and the maximum edge length of the tetrahedron element is usually regarded as the maximum length. According to the above empirical formulas, and considering the actual calculation speed and calculation accuracy of the model, the model element size was set to 1.0 m.

Boundary conditions and model parameters

In the calculation, the static boundary was adopted at the bottom of the model, surrounded by the free field boundary (Fig. 6a), which is used to absorb the incident wave and avoid the influence of boundary conditions. To make the stress state of the free field model and the roadway model consistent, the initial equilibrium calculation of the free field boundary was performed, and the same stress wave was applied to the free field boundary on the right side of the model during dynamic analysis. According to the measured in-situ stress data, the initial stress condition was imposed on the boundary of the model. Under the action of self-weight stress and tectonic stress, the model first reached the initial stress equilibrium state, and then the impact stress wave was applied. In the dynamic response analysis, the stress wave loading program written with FISH statement embedded in 3DEC was used to apply the left horizontal incident semi-sinusoidal stress wave (Fig. 6b) to the right side of the model to simulate the impact disturbance on the surrounding rock of the roadway. It was estimated that the peak value of the impact stress wave was about 15.02 MPa and the frequency was 20 Hz. The stress wave action time was set to 0.1 s, during which the dynamic response of the surrounding rock of the roadway can be completed (Lu et al. 2008).

Fig. 6

The damping in the model calculation is selected as localized damping, and the damping coefficient is 0.15. Since the 3DEC model block is a deformable body, the linear elastic model was used for the rock mass in the initial equilibrium calculation, the Mohr-Coulomb strength criterion was adopted in the stress wave dynamic calculation, and the Coulomb slip model was used for the joint surface. As the simulation section of the roadway has not been effectively supported in the actual project, the influence of the supporting structure is not considered in the entire simulation calculation process.

According to the results of laboratory tests, the mechanical parameters of rock mass used in the numerical simulation calculation of jointed rock roadway are shown in Table 2. In the 3DEC simulation, there is no uniform standard for the values of joint parameters. Because it is difficult to determine the mechanical parameters of joints according to experiments, most of the mechanical parameters are approximately determined based on simulation experience and engineering analogy. In this study, based on the selection method of mechanical parameters of jointed rock mass introduced by Jin (2013), and assuming that the mechanical parameters of the two groups of joints added to the model are the same, the obtained joint mechanical parameters are presented in Table 3.

Table 2

Table 3

Numerical simulation results analysis

Deformation evolution characteristics

The stability of the roadway surrounding rock will be directly reflected in the deformation of the roadway surrounding rock. After roadway excavation, the deformation displacement and plastic zone obtained after initial equilibrium are cleared, and then the dynamic analysis of impact stress wave loading is carried out. Fig. 7 manifests the vertical displacement evolution of the right side of the surrounding rock of the jointed rock roadway under impact disturbance. For the convenience of comparison, the absolute value of displacement is adopted. It can be found that under the impact stress wave, the surrounding rock of the roadway is deformed, the roof of the roadway moves downward, the floor of the roadway moves upward, and the vertical displacement range extends to the two sides of the roadway. The block slides along the joint plane, showing an obvious joint influence effect. With the increase of impact stress wave action time, the range and magnitude of vertical displacement of roadway roof and floor gradually increase. The maximum vertical displacement of the roadway roof is 7.08 cm, and the maximum deformation occurs from the center of the roadway roof to the upper right corner. The maximum vertical displacement of the roadway floor is 9.54 cm, and the maximum deformation occurs in the lower right corner of the roadway floor, which may be caused by the local stress concentration induced by the impact on the right side of the roadway. Overall, the deformation of the roadway floor is relatively small except for the lower right corner. The range and average value of the deformation increasing area of roadway roof are larger than that of roadway floor, which is because the surrounding rock of roadway is damaged after impact disturbance, and the roadway roof moves to the free surface under the action of gravity, resulting in a larger overall displacement of roadway roof. Besides, the maximum deformation area of the roadway roof and floor are inclined to the right side of the roadway, which is caused by impact disturbance on the right side of the roadway.

Fig. 7

Fig. 8 presents the evolution of horizontal displacement when the right side of the surrounding rock of the jointed rock roadway is disturbed by the impact. It can be observed that under the impact stress wave, both sides of the roadway are compressed inward. With the increase of impact stress wave action time, the horizontal displacement of both sides of the roadway increases gradually. The maximum deformation of the right side of the roadway is approximately 11.75 cm, and the maximum deformation occurs in the middle and lower part of the right side of the roadway. The maximum deformation of the left side is about 9.92 cm, and the maximum deformation occurs in the upper part of the left side. The maximum horizontal displacement on the right side of the roadway is greater than that on the left side of the roadway due to the impact disturbance on the right side of the roadway. In addition, the range and magnitude of the horizontal displacement of the two sides of the roadway are larger than that of the vertical displacement of the roof and floor, which indicates that the damage degree of the two sides of the roadway caused by impact disturbance is greater than that of the roof and floor, and the deformation damage is more serious. It should be noted that the displacement of roadway surrounding rock in the calculation results of the model is slightly larger because of the large deformation of the block and the existence of joints in the discrete element program.

Based on the above analysis, due to the existence of joints, the joint plane first slips after impact disturbance, and the deformation of both sides and roof and floor of roadway slips along the joint plane, which indicates that the impact disturbance of roadway will lead to a certain degree of dislocation failure of rock mass along the weak plane of the structure, and the deformation of different areas is different. The fracture surface formed by joint slip is a small-fault with displacement barrier effect and local amplification effect (Liu et al. 2019). Compared with the roadway free face, the deep surrounding rock is less affected by impact disturbance and

the deformation is smaller. In a word, the existence of joints has an important influence on the stability of the roadway surrounding rock. The deformation is concentrated in the area between the weak surface of the structure and the roadway, and the stability of the roadway becomes worse.

Fig. 8

Additionally, the displacement of the key parts of roadway deformation (Fig. 9a) was monitored during the simulation. Fig. 9b shows the recorded evolution characteristics of vertical displacement at the center points of the roof and floor of the roadway and horizontal displacement at the center points of the left and right sides of the roadway, all of which are absolute values. It can be found that the deformation laws displayed by the four monitoring points are quite consistent. In the dynamic calculation time range, the displacement increases with the increase of the impact stress wave action time, which increases slowly in the initial stage and increases approximately linearly in the later stage. Generally, the deformation values of the four monitoring points are the right center, left center, top plate center, and bottom plate center from large to small, and the displacements of left-center and roof center are relatively close. Because the right side of the roadway is disturbed by impact, the damage degree in the horizontal direction is larger than that in the vertical direction overall.

Fig. 9

Evolution characteristics of the plastic zone

Fig. 10 manifests the evolution contours of the plastic zone when the right side of the surrounding rock of the jointed rock roadway is disturbed by the impact. Different colors represent different failure states. The plastic zone first appears on the right side of the roadway, indicating that the deformation and failure first occur on the right side of the roadway. With the increase of impact stress wave action time, the plastic zone around the roadway expands from the free surface to the deep surrounding rock, and the plastic zone area gradually increases. The area of the plastic zone in different parts of the roadway is different. The area of the plastic zone on the right side of the roadway is slightly larger than that on the left side, mainly concentrated in the upper right corner and lower right corner of the roadway. In the later stage of impact disturbance, the surrounding rock of the roadway begins to be destroyed in a certain range. Tension-shear failure mainly occurs in a small range close to the roof and floor of the roadway and the free faces of the two sides, and tensile failure occurs locally, while shear failure mainly occurs along the joint plane outside this range. In other words, there are three failure modes in the surrounding rock of jointed rock roadway: tensile-shear failure, tensile failure, and shear failure, which is similar to the failure modes of randomly jointed circular roadway (Fig. 11) obtained by Liu et al. (2019). But overall, the main failure mode of the jointed rock roadway is the shear failure.

Fig. 10

Fig. 11

In conclusion, when the joints in the surrounding rock of the roadway are well-developed, the stability of the roadway decreases greatly. After being disturbed by the impact, the sliding dislocation area of the surrounding rock along the joint plane and the shear cracking range of the joints increases significantly. In addition, with the increase of impact stress wave action time, the plastic area of the two sides and roof and floor of roadway gradually increases, and the risk of failure increases. Due to the existence of joints and impact disturbance, the deformation and stress level of surrounding rock of the two sides and roof and floor of roadway gradually increase, and the degree of instability and failure tends to be serious. The joints cut the surrounding rock of the roadway, which makes the surrounding rock of the roadway form an unstable structure, and easy to form local stress concentration, so it becomes a more vulnerable part to failure. In particular, the deformation and stress level of the area where the dominant joints are located are relatively large on the right side of the roadway, and disasters such as spalling, spalling, and collapse may occur preferentially after being disturbed by impact, which is similar to the failure of the surrounding rock of the roadway in the actual engineering site (Fig. 12). Therefore, based on the existing supporting structure, local support should be strengthened in the joint and fissure development area of the roadway. Moreover, the numerical simulation results based on structural plane investigation and in-situ stress measurement in this study well reflect the failure characteristics of roadway surrounding rock in the engineering field, which can provide a scientific basis for future roadway support.

Fig. 12

Factors influencing the dynamic stability of the surrounding rock of jointed rock masses

To further explore the influencing factors of the dynamic stability of the surrounding rock of the jointed rock mass, three major influencing factors of buried depth, stress wave peak value, and stress wave delay were selected in this study. By setting different values of the above factors, sensitivity analysis of a single influencing factor was adopted.

Buried depth

A large-scale gold deposit has been found at a depth of about 2000 m underground in the mine, which will continue to be mined deep in the future. To further study the evolution law of deformation and plastic zone of roadway surrounding rock in jointed rock mass under different buried depths, the roadway buried depth was selected as 1200 m, 1400 m, 1600 m, 1800 m, and 2000 m, and the load was applied in the form of the half-sine stress wave. The peak value of the impact stress wave was set as 15.02 MPa, the frequency of the impact stress wave was 20 Hz, and the dynamic calculation time was 0.1 s. Using the jointed rock roadway model established in the previous section, the mechanical parameters of jointed rock mass were unchanged. According to the obtained in-situ stress field model, the in-situ stress values of corresponding depths were calculated, and the real stress boundary conditions were applied to the numerical model to analyze the dynamic stability of various buried tunnels under the same dynamic disturbance.

Figs. 13–14 show the deformation of surrounding rock of jointed rock roadway under different buried depths after impact disturbance. The maximum vertical displacement of roadway roof is 11.01 cm when the buried depth is 1200 m, and the maximum vertical displacement of roadway roof is 13.34 cm, 15.80 cm, 17.65 cm, and 20.36 cm when the buried depth is 1400 m, 1600 m, 1800 m, and 2000 m, respectively, which increases by 21.16%, 30.32%, 60.31%, and 84.92% compared with 1200 m. The maximum vertical displacement of roadway floor is 13.43 cm when the buried depth is 1200 m, and the maximum vertical displacement of roadway floor is 15.32 cm, 17.08 cm, 19.20 cm, and 22.70 cm when the buried depth is 1400 m, 1600 m, 1800 m, and 2000 m, respectively, showing an increase of 14.07%, 27.18%, 42.96%, and 69.02%, respectively. The maximum horizontal displacement of the left side of the roadway is 11.98 cm when the buried depth is 1200 m, and the maximum horizontal displacement of the left side of the roadway is 14.98 cm, 21.10 cm, 29.28 cm, and 40.65 cm when the buried depth is 1400 m, 1600 m, 1800 m, and 2000 m, respectively, increasing by 25.04%, 76.13%, 144.41%, and 239.32% compared with 1200 m. The maximum horizontal displacement of the right side of the roadway is 16.87 cm when the buried depth is 1200 m, and the maximum horizontal displacement of the right side of the roadway is 22.24 cm, 23.12 cm, 23.94 cm, and 25.54 cm when the buried depth is 1400 m, 1600 m, 1800 m, and 2000 m, respectively, which increases by 31.83%, 37.05%, 41.91%, and 51.39% compared with 1200 m. It can be found that under the same impact disturbance, with the increase of roadway buried depth, the inward extrusion deformation of two sides of the roadway, the subsidence of roof, and the floor heave increase gradually. It should be noted that the maximum horizontal displacement value of the left side of the roadway increases sharply with the increase of buried depth, which exceeds the maximum horizontal displacement value of the right side of the roadway. This is because small blocks are extruded from the left side of the roadway, resulting in a substantial increase in its maximum displacement value. Meanwhile, this phenomenon shows that the disturbance effect of impact load with the same strength is different due to the different stress states of the surrounding rock. Overall, the deformation of the whole area of the right side of the roadway is still greater than that of the left side. The deep surrounding rock far away from the free face of the roadway is weakly affected by impact disturbance and has little deformation. Besides, the displacement of surrounding rock of jointed rock roadway calculated by simulation in this study is similar to that obtained by Wang (2014).

Fig. 15 displays the evolution characteristics of vertical displacement at the center points of the roof and floor of the roadway and horizontal displacement at the center points of the left and right sides of the roadway under different burial depths, and the displacements are absolute values. It can be seen from Figs. 15a–e that the deformation laws displayed by the four monitoring points under different burial depths are generally similar. In the time range of dynamic calculation, with the increase of the impact stress wave action time, the displacement increases gradually, which increases slowly in the initial stage and increases approximately linearly in the later stage. As shown in Fig. 15f, with the increase of buried depth, the maximum values of vertical displacement and horizontal displacement of monitoring points increase. From 1200 m to 2000 m, the vertical displacement at the center points of roof and floor and the horizontal displacement at the center points of left and right sides of roadway increase by 59.09%, 60.00%, 56.70%, and 55.38%, respectively, showing that the increase of the floor displacement is relatively large. Under the same buried

depth, the deformation values of the four monitoring points in the roadway are right side center, roof center, left side center, and floor center in order from large to small, which is slightly different from the actual deformation at the depth of 915 m, and the displacement of left side center and roof center is close. Because the right side of the roadway is disturbed by impact, it is further confirmed that the damage degree in the horizontal direction is larger than that in the vertical direction at each buried depth.

Fig. 13

Fig. 14

Fig. 15

According to the above analysis, under the same buried depth, the inward extrusion deformation of the two sides of the roadway is larger than the subsidence of the roof and the floor heave after the impact disturbance. The displacement of roadway surrounding rock increases with the increase of roadway buried depth, i.e., the greater the buried depth, the larger the deformation of the roadway. The displacement change rate of roof and floor of roadway is roughly the same, while the displacement change rate of the left side of the roadway is relatively large and that of the right side is relatively small. In summary, under different buried depth conditions, because the right side of the roadway is disturbed by horizontal impact, the impact disturbance has a significant impact on the two sides of the surrounding rock of the roadway, which tends to cause dynamic instability such as side deviation, spalling, and rockburst. At the same time, the deformation of the two sides will also cause the deformation of the roof and floor. Therefore, effective support and reinforcement measures should be taken to control the deformation of the two sides and the roof and floor in deep mining in the future to ensure the overall stability of the surrounding rock of the jointed rock roadway.

After the impact disturbance, the damage range of roadway surrounding rock under different buried depths increases significantly with the increase of stress wave action time. Fig. 16 manifests the failure characteristics of surrounding rock of jointed rock roadway under different buried depths. With the increase of roadway buried depth, the plastic zone of roadway surrounding rock expands from the free surface to the deep part of surrounding rock, and the range of plastic zone shows an increasing trend, but the increase is small. Under different burial depths, the failure characteristics of roadway surrounding rock are similar. Tension-shear failure mainly occurs in a small range close to the roof and floor of the roadway and the free faces of the two sides, and tensile failure occurs locally, while shear failure mainly occurs along the joint plane outside this range. Therefore, due to the existence of joints, shear failure mainly occurs in the surrounding rock of the roadway. In addition, in the range of study depth, the change of plastic zone of surrounding rock of roadway is gradual after the impact disturbance, that is, the plastic zone is gradually destroyed from the free face to the deep part of the surrounding rock. In general, the right side of the roadway with different buried depth shows similar fracture morphology after impact disturbance, but with the increase of buried depth, the damage degree is aggravated.

Fig. 16

Peak stress wave

The roadway may be disturbed by different stress wave peaks during service. To study the evolution law of deformation and plastic zone of roadway surrounding rock of jointed rock masses under different stress wave peaks, the buried depth of roadway was fixed at 1600 m, the loading mode of semi-sinusoidal stress wave was adopted, the impact stress wave frequency was 20 Hz, the stress wave peaks were 5 MPa, 10 MPa, 15.02 MPa, 20 MPa, and 25 MPa, and the dynamic calculation time was 0.1 s. The dynamic stability of the same roadway under different stress wave peak disturbance was analyzed using the jointed rock roadway model with the same mechanical parameters.

Figs. 17–18 show the deformation and failure characteristics of roadway surrounding rock under different peak values of the impact stress wave. The larger the peak value of the stress wave, the higher the corresponding disturbance level. With the increase of stress wave peak value, the inward extrusion deformation, roof subsidence, and floor heave of roadway surrounding rock gradually increase. The maximum vertical displacement of roadway roof is 13.22 cm when stress wave peak value is 5 MPa, and the maximum vertical displacement of roadway roof is 15.76 cm, 15.80 cm, 15.89 cm, and 20.46 cm when the peak stress wave is 10 MPa, 15.02 MPa, 20 MPa, and 25 MPa, respectively, which increases by 19.21%, 19.52%, 20.20%, and 54.77% compared with 5 MPa. The maximum vertical displacement of roadway floor is 14.91 cm when the peak stress wave is 5 MPa, and the maximum vertical displacement of roadway floor is 17.54 cm, 17.08 cm, 20.82 cm, and 20.88 cm when the peak stress wave is 10 MPa, 15.02 MPa, 20 MPa, and 25 MPa, respectively, increasing by 17.64%, 14.55%, 39.44%, and 40.04% compared with 5 MPa. The maximum horizontal displacement of the left side of the roadway is 14.93 cm when the stress wave peak value is 5 MPa, and the maximum

horizontal displacement of the left side of the roadway is 17.71 cm, 21.10 cm, 28.51 cm, and 30.95 cm respectively, when the stress wave peak value is 10 MPa, 15.02 MPa, 20 MPa, and 25 MPa, respectively, showing an increasing of 18.62%, 41.33%, 90.96%, and 107.30%, respectively. The maximum horizontal displacement of the right side of the roadway is 19.13 cm when the stress wave peak value is 5 MPa, and the maximum horizontal displacement of the right side of the roadway is 21.81 cm, 23.12 cm, 22.28 cm, and 25.10 cm, respectively, when stress wave peak value is 10 MPa, 15.02 MPa, 20 MPa, and 25 MPa, respectively, which increases by 14.01%, 20.86%, 16.47%, and 31.21% compared with 5 MPa. Hence, the deformation characteristics of the surrounding rock of the roadway are different after the disturbance of different stress wave peaks, and the deformation of the right side of the roadway is relatively large. With the increase of stress wave peak value (disturbance level), the subsidence of roadway roof, floor heave, and inward extrusion deformation of two sides all increase gradually. This is because the greater the stress wave peak value, the higher the input stress wave energy, resulting in the greater cumulative damage of roadway surrounding rock joint surface and more serious deformation of surrounding rock. In general, the deformation of deep surrounding rock far away from the roadway free face is small.

Fig. 19 presents the evolution characteristics of vertical displacement at the center points of the roadway roof and floor and horizontal displacement at the center points of the left and right sides of the roadway under different stress wave peak conditions, and the displacements are absolute values. It can be seen from Figs. 19a–e that the deformation laws displayed by the four monitoring points under different stress wave peaks are generally similar. In the time range of dynamic calculation, with the increase of impact stress wave action time, the displacement of monitoring points increases gradually, which increases slowly in the initial stage and increases approximately linearly in the later stage. As seen from Fig. 19f, with the increase of stress wave peak value, the maximum values of vertical displacement and horizontal displacement of monitoring points increase. The vertical displacement at the center points of roof and floor and the horizontal displacement at the center points of the left and right sides of the roadway is 12.39 cm, 8.21 cm, 11.28 cm, and 14.72 cm respectively when the stress wave peak value is 5 MPa. The vertical displacement at the center points of roof and floor and the horizontal displacement at the center points of the left and right sides of roadway is 18.24 cm, 13.21 cm, 15.52 cm, and 21.33 cm respectively, increasing by 47.22%, 60.90%, 37.59%, and 44.90% respectively, indicating that the displacement increment of roadway floor is relatively large. Under different stress wave peak disturbance conditions, the disturbance deformation of roadway surrounding rock shows a similar law. Under the same stress wave peak value, the deformation values of four monitoring points of roadway are right side center point, roof center point, left side center point and floor center point in order from large to small, and the displacements of left side center point and roof center point are relatively close. In addition, the deformation degree of roadway in the horizontal direction is larger than that in the vertical direction overall, which is similar to the deformation situation under different buried depths.

Fig. 17

Fig. 18

Fig. 19

Fig. 20 presents the failure characteristics of surrounding rock of jointed rock roadway under different stress wave peak conditions. With the increase of peak value of impact stress wave, the plastic zone area of surrounding rock of roadway increases, but the increase is limited. There are three failure modes of roadway surrounding rock, i.e., tensile failure, tensile-shear failure, and shear failure, and the shear failure is the main failure mode, which may be because stress waves acting on the surrounding rock of jointed rock roadway will induce preferential shear slip of joint plane. Under the peak stress wave conditions, the tensile failure and tensile-shear failure areas are close to the roadway free face and occupy a small area. The shear failure area is mainly outside the tensile failure area and tensile-shear failure area, which occupies a large area.

Fig. 20

In addition, under the disturbance of different stress wave peak conditions, with the increase of stress wave peak value, the damage degree of roadway surrounding rock becomes more serious, and the sliding of small blocks in roadway roof and floor and two sides along the joint face is more significant, which indicates that the energy released by the failure of roadway surrounding rock under the condition of higher stress wave peak value is larger, and also means that the intensity of impact disaster will increase to some extent.

Stress wave delay

To analyze the evolution law of surrounding rock deformation and plastic zone in jointed rock roadway under different stress

wave delay conditions, the buried depth of roadway was fixed at 1600 m, the loading mode of semi-sinusoidal stress wave was adopted, the peak value of stress wave was set at 15.02 MPa, the dynamic load frequency was selected as 5 Hz, 10 Hz, 20 Hz, 30 Hz, and 40 Hz, and the dynamic calculation time was 0.1 s. The dynamic stability of the same roadway under different stress wave delay disturbance was analyzed using the jointed rock roadway model with the same mechanical parameters.

Figs. 21–22 show the deformation characteristics of the surrounding rock of jointed rock roadway under different stress wave delay conditions. The lower the frequency, the longer the stress wave delay. With the increase of stress wave delay, the subsidence of roof and floor heave of roadway surrounding rock decrease, and the inward extrusion of side increases. The maximum vertical displacement of the roadway roof is 15.81 cm when the stress wave frequency is 40 Hz, and 15.87 cm, 15.80 cm, 15.83 cm, and 15.75 cm when the stress wave frequency is 30 Hz, 20 Hz, 10 Hz, and 5 Hz, respectively. The maximum deformation of the roof under different stress wave delay is the same. The maximum vertical displacement of the roadway floor is 52.64 cm when the stress wave frequency is 40 Hz, and 17.71 cm, 17.08 cm, 17.35 cm, and 17.33 cm when the stress wave frequency is 30 Hz, 20 Hz, 10 Hz, and 5 Hz, respectively. Compared with the frequency of 40 Hz, the maximum displacement of the roadway floor is greatly reduced, which is due to the small block sliding out when the frequency is 40 Hz. The maximum horizontal displacement of the left side of the roadway is 44.05 cm when the stress wave frequency is 40 Hz, and 16.82 cm, 21.10 cm, 19.26 cm, and 29.43 cm when the stress wave frequency is 30 Hz, 20 Hz, 10 Hz, and 5 Hz, respectively. With the decrease of the frequency, the maximum horizontal displacement first decreases and then increases. The maximum horizontal displacement of the right side of the roadway is 22.54 cm when the stress wave frequency is 40 Hz, and 21.22 cm, 23.12 cm, 21.82 cm, and 21.52 cm when the stress wave frequency is 30 Hz, 20 Hz, 10 Hz, and 5 Hz, respectively, implying that the maximum deformation of the right side under different stress wave delays has little difference. In addition, the deformation of the roadway surrounding rock is mainly concentrated near the free face of the roadway, and the deep surrounding rock of the roadway is weakly affected by impact disturbance, and the displacement is small.

Fig. 23 plots the evolution characteristics of vertical displacement at the center points of the roof and floor of the roadway and horizontal displacement at the center points of the left and right sides of the roadway under different stress wave delay conditions. The displacements are absolute values. It can be observed from Figs. 23a–e that the deformation laws displayed by the four monitoring points under different stress wave delays are generally similar. In the time range of dynamic calculation, with the increase of impact stress wave action time, the displacement of monitoring points increases gradually, which increases slowly in the initial stage and rapidly in the later stage, showing an approximately linear increase, which is similar to the deformation law under different buried depths and different stress wave peaks. Moreover, as shown in Fig. 23f, with the increase of stress wave delay, the maximum values of vertical displacement and horizontal displacement of monitoring points decrease. When the stress wave frequency is 40 Hz, the vertical displacement at the center points of roof and floor and the horizontal displacement at the center points of the left and right sides of roadway is 15.01 cm, 9.80 cm, 13.79 cm, and 20.31 cm respectively. When the stress wave frequency is 5 Hz, the vertical displacement at the center points of roof and floor and the horizontal displacement at the center points of the left and right sides of roadway is 13.70 cm, 7.51 cm, 12.32 cm, and 15.30 cm, respectively, which decreased by 8.73%, 23.37%, 10.66%, and 24.67%, showing that the displacement decrease of the floor and right sides of roadway is relatively large. Moreover, under different stress wave delay disturbance conditions, the disturbance and deformation laws of roadway surrounding rock are relatively consistent. Under the same stress wave delay, the deformation values of four monitoring points of roadway are right side center point, roof center point, left side center point and floor center point in order from large to small, and the displacements of left side center point and roof center point are relatively close. Under various stress wave delay conditions, the deformation degree of roadway in the horizontal direction is larger than that in the vertical direction overall, which is similar to the deformation conditions under different buried depths and different stress wave peaks.

Fig. 21

Fig. 22

Fig. 23

Fig. 24 illustrates the failure characteristics of surrounding rock of jointed rock roadway under different stress wave delay conditions. When the surrounding rock of the jointed rock roadway is disturbed by impact, a stress concentration zone will be formed at the joint tip or joint surface. When the stress of surrounding rock in the stress concentration zone exceeds the strength of surrounding rock, the plastic zone will expand and the surrounding rock of roadway will slip. It can be observed that with the

increase of stress wave delay (the frequency decreases), the plastic zone area of roadway surrounding rock increases slightly, but the increase is not significant. Under the influence of different impact stress wave disturbance delays, tensile-shear failure mainly occurs in a small range of roadway free face, and tensile failure occurs locally, while shear failure mainly occurs along the joint plane outside this range. Combined with the whole deformation characteristics of roadway surrounding rock, it can be found that with the increase of stress wave delay, the damage degree of the roof and right side of roadway has no obvious change, the damage degree of the floor is weakening overall, and the damage degree of the left side is weakening at first and then increasing. When the stress wave frequency is 40 Hz and 5 Hz, some small blocks protrude from the left side of the roadway.

Fig. 24

By analyzing the practical engineering case and dynamic stability of surrounding rock of jointed rock roadway under different influencing factors, it can be seen that when the right side of the roadway is disturbed by impact, the impact tendency of the right side of the roadway is significantly affected, and the deformation of the right side of the roadway is the largest, followed by the roof, and the deformation of the left side and the bottom plate is relatively small, which can better reflect the failure characteristics of surrounding rock of jointed rock roadway in practical engineering. Overall, the failure process of surrounding rock of jointed rock roadway can be summarized as follows: stress concentration firstly occurs in the surrounding rock of the right side of the roadway, and then it extends to the whole roadway, with the block sliding along the joint plane or the block breaking, and the sliding failure area of surrounding rock increases, resulting in the release of stress wave energy, which eventually leads to discontinuous deformation of roadway surrounding rock and significant inward convergence as a whole. Furthermore, from the influence degree of buried depth, stress wave peak, and stress wave delay on the deformation and failure of surrounding rock of jointed rock roadway, it can be found that buried depth and peak stress wave have a great influence on the dynamic stability of surrounding rock of jointed rock roadway (displacement variation is relatively large), while the stress wave delay has little influence (displacement variation is relatively small), but the influence result is complicated. Therefore, for the dynamic stability of jointed rock roadway in practical engineering, it is necessary to comprehensively analyze the main influencing factors and reasonably evaluate its stability according to the specific engineering conditions.

The impact failure mechanism of the surrounding rock in jointed rock masses

The cause and evolution of instability and failure of surrounding rock of jointed rock roadway are important engineering problems, which involves the mechanical mechanism to control the stability of rock mass. The existence of joints destroys the integrity of the surrounding rock of the chamber, greatly reduces the strength of rock mass, and changes the stress distribution pattern in the surrounding rock of the chamber. High-stress concentration is often formed at the joint tips and the intersection of cross joints. According to rock damage fracture mechanics, the joint plane forms a weak spatial structure in the surrounding rock of the chamber, which increases the stress concentration, promotes the initiation and propagation of cracks, and makes the deformation characteristics and stress distribution more complex. The gradual and sudden failure process of the surrounding rock of jointed rock masses under static and dynamic loads can be divided into multiple evolution stages, although the duration of the failure process varies greatly. Essentially, the macroscopic failure of the surrounding rock chamber is the cumulative reflection of the initiation and propagation of microcracks in the surrounding rock.

The above numerical simulation results show that the existence of joints reduces the stability of the roadway and makes the response of the roadway more sensitive and violent to external disturbance. When the surrounding rock of the jointed rock roadway is disturbed by impact, its instability and failure process transits from a gradual change in the early stage to sudden instability. The gradual failure of surrounding rock indicates that the block in surrounding rock slides stably along the joint plane in the early stage, and shows the limited-slip process of macroscopic fracture plane in the later stage, while the unstable failure stage of surrounding rock indicates the acceleration of dislocation of the subcritical joint plane, which eventually leads to instability and failure of the roadway. When the right side of the surrounding rock of the jointed rock roadway is disturbed by impact, the deformation of the surrounding rock shows remarkable inhomogeneity. The maximum horizontal deformation is located on the right side of the roadway and the maximum vertical deformation is located on the floor of the roadway. With the increase of impact disturbance intensity, the non-uniformity characteristics of this deformation become more prominent, which will lead to the non-uniform damage of roadway, and it is easy to cause local severe damage. Once a large amount of energy is rapidly accumulated in the local surrounding rock,

which is greater than the energy required for its fracture, sudden damage will occur, such as rockburst. Under the impact disturbance, the surrounding rock of the jointed rock roadway is mainly characterized by shear stress concentration and local tensile stress concentration. Because the tensile strength of rock is generally far lower than the compressive strength, the position of tensile stress in the surrounding rock will be destroyed first. Under the impact stress wave, the instability and failure modes of roadway are complex, the inward extrusion deformation of two sides of roadway is serious, the roof drops greatly, the floor bulges seriously, and the roadway shows overall convergence and deformation failure. The surrounding rock of the roadway slips into the roadway, and the surrounding joint surfaces also crack and slip further, until the overall failure of the roadway occurs.

During the construction or service of the roadway, when the impact wave from a certain direction, such as blasting operation, earthquake, and rockburst, disturbs the roadway, the dynamic stress wave interacts and superposes with the static stress field on the surrounding rock, resulting in a sudden and significant increase in the stress level in the surrounding rock. In the process of propagation, stress waves are accompanied by energy transmission, and the energy carried by stress waves tends to be released to the weak positions. For the joint surface on the impact side (the right side of the roadway in this study), the existence of the roadway makes its guiding effect more significant and the stress more concentrated. After the impact disturbance, the right joint surface first responds to the impact disturbance, and the block near the roadway free face slips along the joint surface. Stress wave propagates to the left side of the roadway by diffraction along the roadway free face and produces dynamic stress concentration around the roadway, which induces the block on the left side of the roadway and the roof and floor to slip to the free face and release energy. Due to the existence of joints, stress waves will be reflected and transmitted many times at the joint plane, and stress waves with different properties will be superimposed at the joint plane, which will further affect the damage degree of the roadway surrounding rock. For the effect of impact disturbance in roadway failure, when the dynamic stress caused by impact disturbance exceeds the concentrated stress of roadway surrounding rock, the impact disturbance plays a leading role in the instability and failure of roadway surrounding rock; otherwise, the impact disturbance plays an inducing role. In addition, factors such as buried depth and stress wave peak will change the stress state of the roadway surrounding rock and aggravate the stress concentration degree at roadway free face. Combined with the deformation and plastic zone characteristics of roadway surrounding rock obtained by simulation, it can be predicted that the most easily damaged part of roadway surrounding rock is the right side. With the increase of buried depth and peak value of impact stress wave, the possibility and intensity of failure will greatly increase.

The deformation and failure mechanism of the surrounding rock of the jointed rock roadway is analyzed from the perspective of deformation and failure characteristics when one side of the jointed rock roadway is disturbed by impact, and the numerical simulation results well reflected the deformation and failure characteristics of roadway. However, due to the small size and high strength of the test sample, the roof falling and floor bulging did not occur. In addition, in the actual production, the roadway may be disturbed by various forms of stress at the same time, and the actual geological structure is extremely complex. The instability and failure mechanism of the surrounding rock of the jointed rock roadway under the comprehensive action of the geological structure, supporting structure, in-situ stress field, and disturbed stress field is more complex, which needs to be further studied.

Generally, when the surrounding rock of the roadway is weakly or not disturbed by the impact, the gradual rock fracture will produce stable tunnel convergence. However, under strong impact disturbances, even after sprayed concrete and/or anchor rods are installed, sudden damage often occurs and shows a sudden displacement curve, as shown in Fig. 25. Therefore, when controlling the instability of surrounding rock of jointed rock masses, targeted technical measures should be taken according to the distribution characteristics of the structural plane, in-situ stress state, and disturbance mechanism of impact stress wave on chamber surrounding rock in specific engineering, so as to change the stress state and supporting structure form of the chamber surrounding rock, weaken the disturbance effect of impact load, and eliminate or reduce the possibility of impact dynamic disaster. In addition, based on the existing supporting structure, local reinforcement support should also be given to the joint and fissure development area and the impact side of the surrounding rock. More importantly, it is necessary to minimize the impact of construction disturbance on the chamber and weaken the disturbance intensity of the impact stress wave propagating to the surrounding rock of the chamber. After determining the reasonable support method, the stability of the surrounding rock should be monitored online in real-time, and the support effect of the chamber should be observed and evaluated so that the support measures can be adjusted in time.

Fig. 25

Conclusions

(1) The in-situ stress magnitudes measured in the gold mine increase linearly with depth. There are two groups of dominant structural planes on the surface of the surrounding rock of the studied roadway. The dominant structural planes of the first and the second groups are 234.24°∠51.04° and 327.47°∠53.89°, respectively, and the average joint spacing is about 0.4 m and 0.3 m, respectively.

(2) The stability of the surrounding rock of the jointed rock roadway is poor. Under the impact stress wave, the surrounding rock of the roadway undergoes overall convergence and deformation. With the increase of impact stress wave action time, the displacements of the two sides and the roof and floor of the roadway gradually increase. The maximum horizontal displacement of the right side of the roadway is greater than that of the left side of the roadway. In addition, the range and magnitude of horizontal displacement of two sides of roadway are larger than that of vertical displacement of roof and floor overall, which indicates that the damage degree of two sides of roadway caused by impact disturbance is greater than that of roof and floor, and the deformation damage is more serious. With the increase of impact stress wave action time, the plastic zone area of surrounding rock of jointed rock roadway increases, and the surrounding rock begins to break in a certain range. There are three failure modes in the surrounding rock: tensile-shear failure, tensile failure, and shear failure. Tensile-shear failure mainly occurs in a small range close to the roof and floor of the roadway and the free surfaces of the two sides, and tensile failure occurs locally, while shear failure mainly occurs along the joint plane outside this range.

(3) Under the same impact disturbance, with the increase of buried depth, the inward extrusion deformation, roof subsidence, and floor heave of the two sides of the roadway gradually increase, and the deformation of the right side of the roadway is relatively large. The deep surrounding rock far away from the free face of the roadway is weakly affected by impact disturbance and has little deformation. The failure area of the surrounding rock extends from the free face to the deep part of the surrounding rock and the range of the plastic zone increases. The right side of the roadway with different buried depth shows similar fracture morphology after being disturbed by impact, while with the increase of buried depth, the degree of damage intensifies.

(4) With the increase of stress wave peak, the deformation of roof and floor and two sides of the roadway increases gradually, and the displacement increment of the roadway floor is relatively large. The larger the peak value of the stress wave, the higher the input stress wave energy, which leads to the greater cumulative damage of the joint surface of the surrounding rock of roadway, thus causing the more serious deformation of the surrounding rock. With the increase of stress wave delay (the frequency decreases), the deformation of roof and floor and two sides of the roadway tends to decrease, the deformation is mainly concentrated near the free face of the roadway, and the deep surrounding rock of the roadway is weakly affected by impact disturbance and has small displacement. The damage degree of the roof and right side of the roadway has no significant change, the damage degree of the floor is weakening overall, while the damage degree of the left side is weakening at first and then increasing.

Acknowledgments This research is financially supported by the State Key Research Development Program of China (No. 2017YFC0804103 and No. 2016YFC0600801) and the National Natural Science Foundation of China (No. 51774022 and No. 52074020).

Conflict of Interest: The authors declare that they have no conflicts of interest.

References

Cai MF, He MC, Liu DY (2002) Rock mechanics and engineering. Science Press, Beijing

Deng XF, Zhu JB, Chen SG, et al (2014) Numerical study on tunnel damage subject to blast-induced shock wave in jointed rock masses. Tunn Undergr Sp Technol 43:88–100. https://doi.org/https://doi.org/10.1016/j.tust.2014.04.004

Han Z, Li D, Zhu Q, et al (2018) Dynamic fracture evolution and mechanical behavior of sandstone containing noncoplanar elliptical flaws under impact loading. Adv Civ Eng 2018:5649357. https://doi.org/10.1155/2018/5649357

Israelsson JI (1996) Short descriptions of UDEC and 3DEC. In: Stephansson O, Jing L, Tsang C-F (eds) Coupled Thermo-Hydro-Mechanical Processes of Fractured Media. Elsevier, pp 523–528

Jin DM (2013) Joint rock tunnel construction process of 3-D numerical simulation analysis. Northeastern University

Li DY, Cheng TJ, Zhou T, Li XB (2015) Experimental study of the dynamic strength and fracturing characteristics of marble specimens with a single hole under impact loading. Chinese J Rock Mech Eng 34:249–260

Li P, Cai M, Guo Q, Miao S (2018) Characteristics and implications of stress state in a gold mine in Ludong area, China. Int J Miner Metall Mater 25:1363–1372. https://doi.org/10.1007/s12613-018-1690-8

Li P, Cai M, Guo Q, Miao S (2019a) In situ stress state of the northwest region of the Jiaodong Peninsula, China from overcoring stress measurements in three gold mines. Rock Mech Rock Eng 52:4497–4507. https://doi.org/10.1007/s00603-019-01827-3

Li P, Ren F, Cai M, et al (2019b) Investigating the mechanical and acoustic emission characteristics of brittle failure around a circular opening under uniaxial loading. Int J Miner Metall Mater 26:1217–1230. https://doi.org/10.1007/s12613-019-1887-5

Li Y, Peng J, Zhang F, Qiu Z (2016) Cracking behavior and mechanism of sandstone containing a pre-cut hole under combined static and dynamic loading. Eng Geol 213:64–73. https://doi.org/https://doi.org/10.1016/j.enggeo.2016.08.006

Liu G, Ma F, Zhao H, et al (2019) Study on the fracture distribution law and the influence of discrete fractures on the stability of roadway surrounding rock in the Sanshandao coastal gold mine, China. Sustainability 11:. https://doi.org/10.3390/su11102758

Lu AH, Yu SL, Qin H, Mao XB (2008) Stability of layered crack structure in roadway surrounding rock under stress wave. J China Univ Min Technol 37:769–774

Lysmer JKRL, Kuhlemeyer RL (1969) Finite dynamic model for infinite media. J Eng Mech Div 95:859–878

Pan YS, Lv XF, Li ZH, Dai SH (2011) Experimental study of dynamic failure process of roadway under high velocity impact loading. Rock Soil Mech 32:1281–1286

Sagong M, Park D, Yoo J, Lee JS (2011) Experimental and numerical analyses of an opening in a jointed rock mass under biaxial compression. Int J Rock Mech Min Sci 48:1055–1067. https://doi.org/https://doi.org/10.1016/j.ijrmms.2011.09.001

Tao M, Ma A, Cao W, et al (2017) Dynamic response of pre-stressed rock with a circular cavity subject to transient loading. Int J Rock Mech Min Sci 99:1–8. https://doi.org/https://doi.org/10.1016/j.ijrmms.2017.09.003

Wang Z (2014) The underground cavern's stability underjoints of the static and dynamic response analysis research. Shandong University

Weng L, Wu Z, Li X (2018) Mesodamage Characteristics of Rock with a Pre-cut Opening Under Combined Static–Dynamic Loads: A Nuclear Magnetic Resonance (NMR) Investigation. Rock Mech Rock Eng 51:2339–2354. https://doi.org/10.1007/s00603-018-1483-4

FIGURES

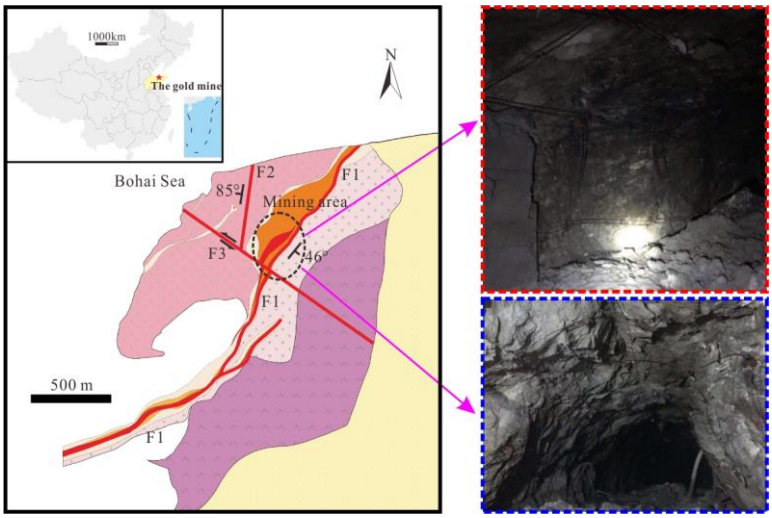

Fig. 1 The geographical location of the gold mine and typical roadway deformation in the local area

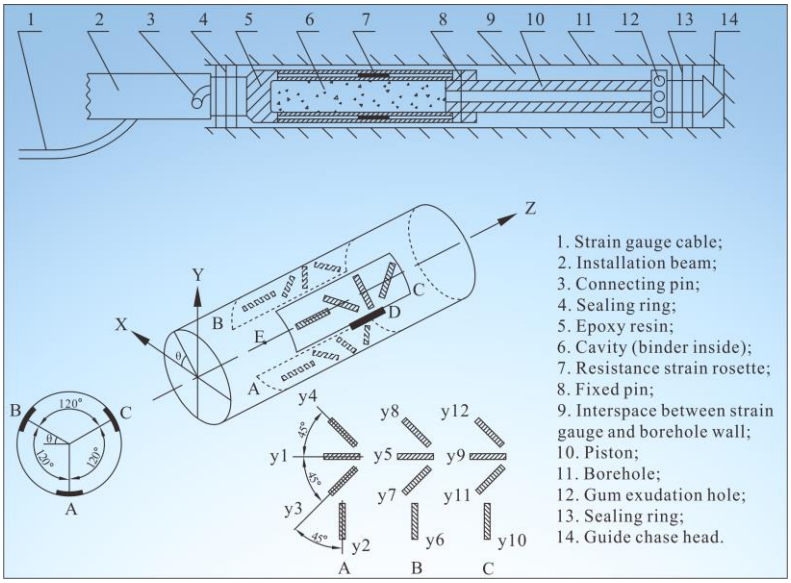

Fig. 2 Schematic diagram of hollow inclusion strain gauge with complete temperature compensation

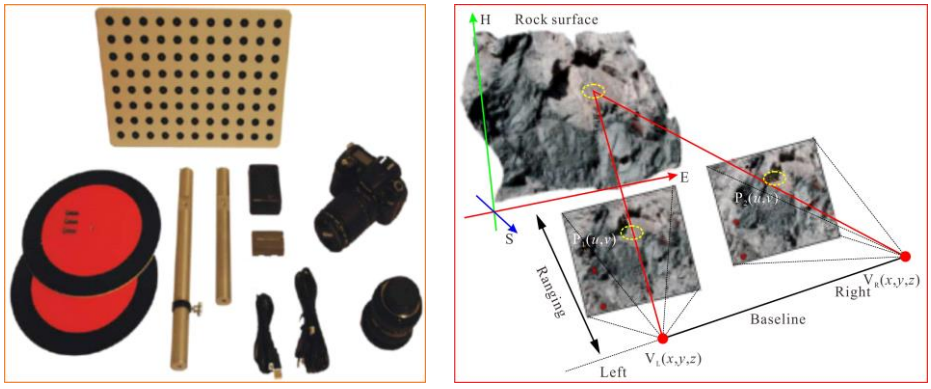

(a) (b)

Fig. 3 Shapemetrix 3D measurement system (a) and the measuring principle of the system (b)

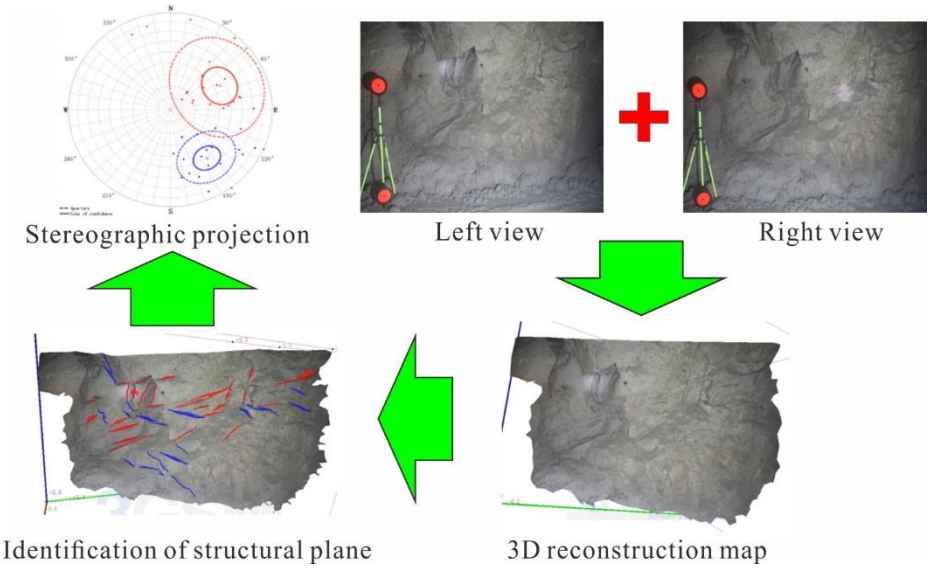

Fig. 4 Illustration of information collection for structural planes of surrounding rock of the roadway

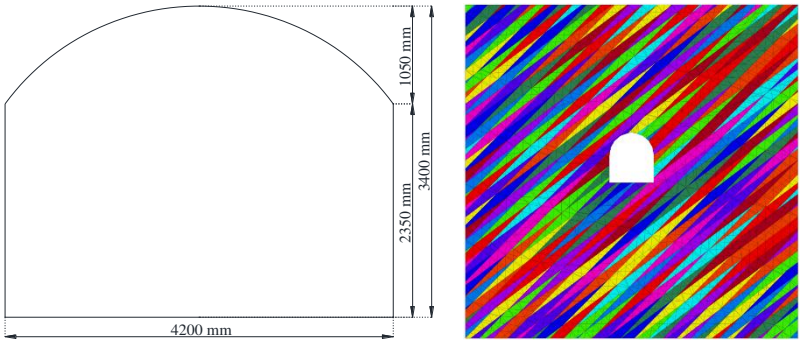

(a) (b)

Fig. 5 Roadway size (a) and plane display of calculation model of jointed rock roadway (b)

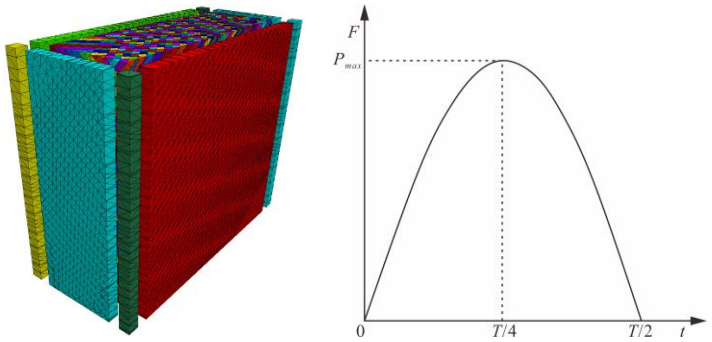

(a) (b)

Fig. 6 Free field boundary (a) and stress wave time history curve (b)

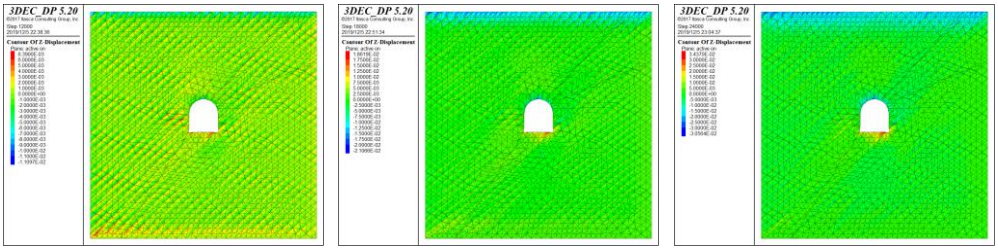

(a) Step 12000 (b) Step 18000 (c) Step 24000

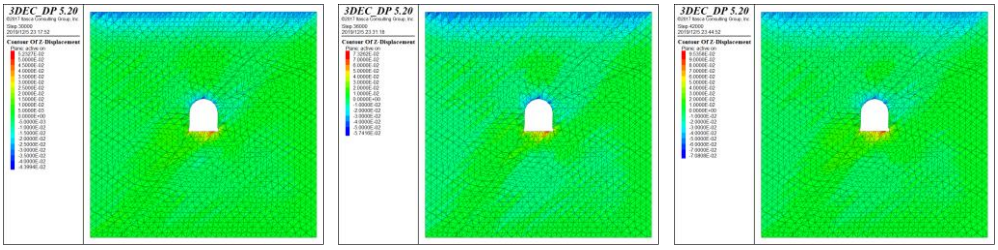

(d) Step 30000 (e) Step 36000 (f) Step 42000

Fig. 7 Vertical displacement evolution contours of the surrounding rock in the jointed rock roadway

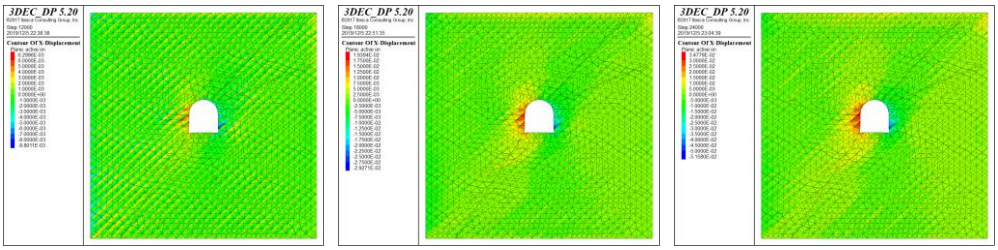

(a) Step 12000 (b) Step 18000 (c) Step 24000

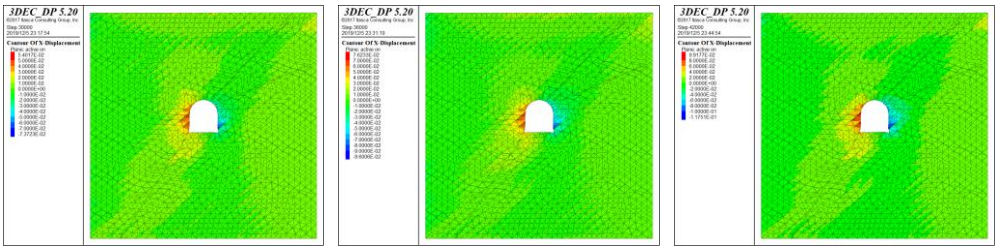

(d) Step 30000 (e) Step 36000 (f) Step 42000

Fig. 8 Horizontal displacement evolution contours of the surrounding rock in the jointed rock roadway

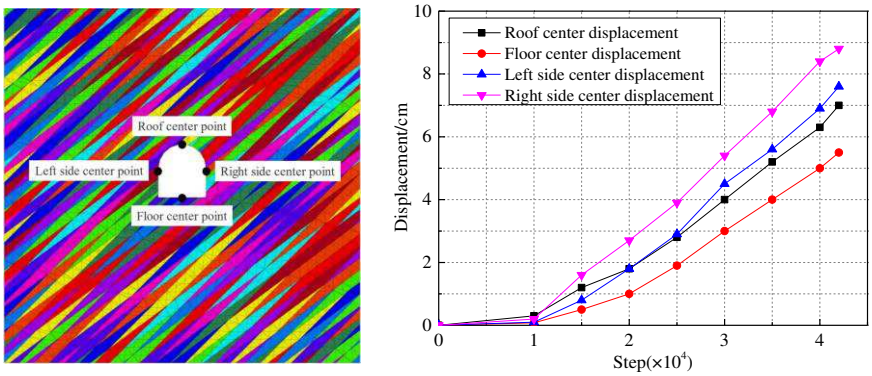

(a) (b)

Fig. 9 Location of monitoring points (a) and displacement of center points of roof, floor, left side, and right side of the roadway (b)

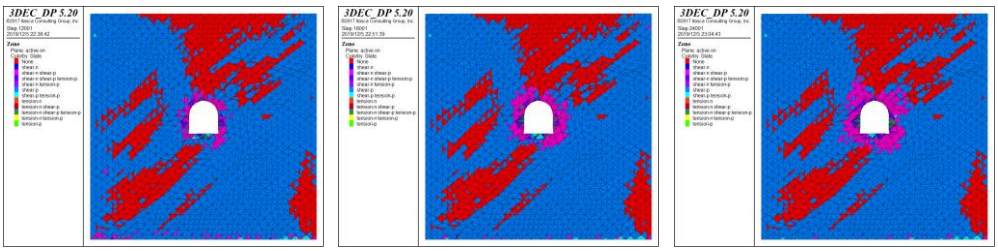

(a) Step 12000 (b) Step 18000 (c) Step 24000

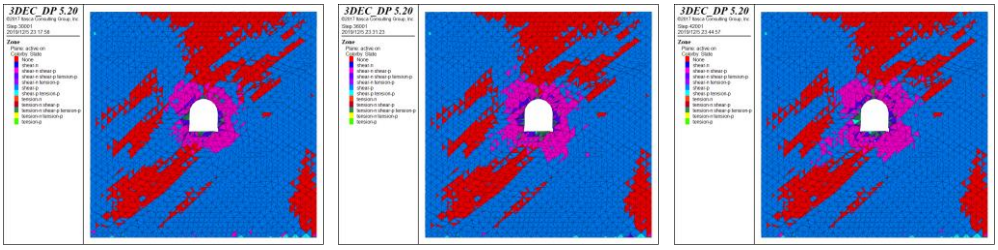

(d) Step 30000 (e) Step 36000 (f) Step 42000

Fig. 10 Evolution contours of the plastic zone of the surrounding rock of jointed rock roadway

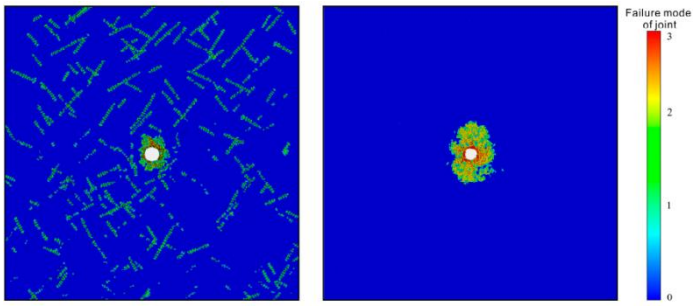

Fig. 11 Failure modes of surrounding rock of random jointed circular roadway (Liu et al. 2019)

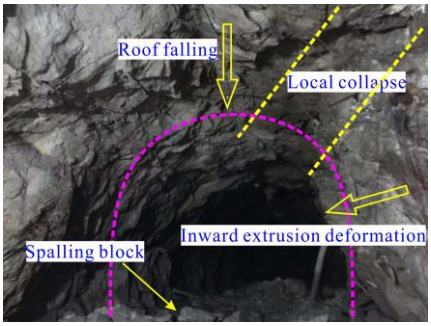

Fig. 12 Deformation and failure of roadway surrounding rock in the engineering field

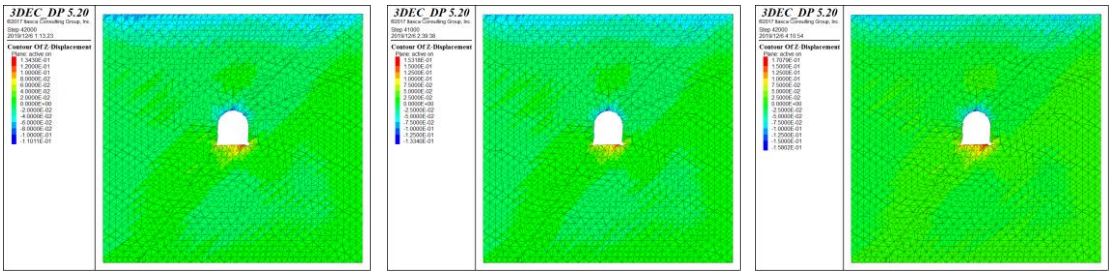

(a) 1200 m (b) 1400 m (c) 1600 m

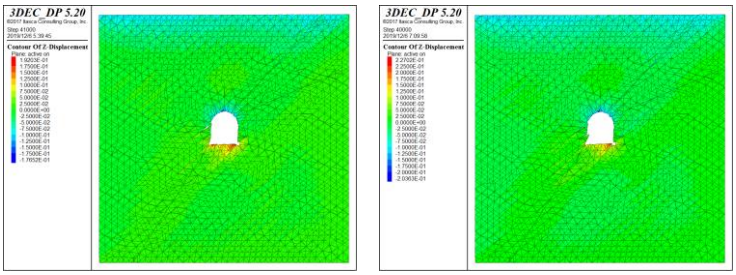

(d) 1800 m (e) 2000 m

Fig. 13 Vertical deformation characteristics of the surrounding rock of jointed rock roadway under different buried depths

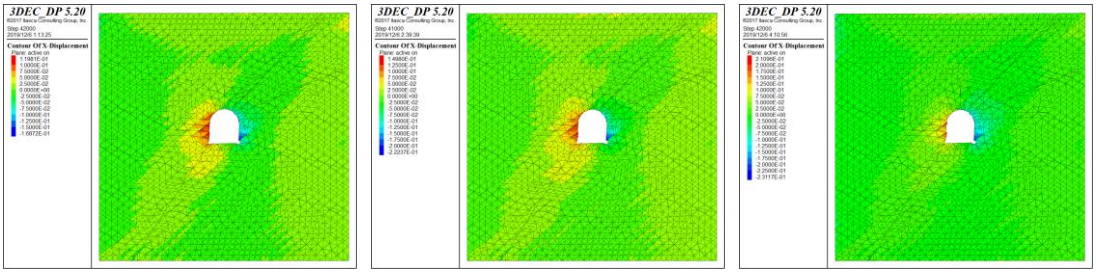

(a) 1200 m (b) 1400 m (c) 1600 m

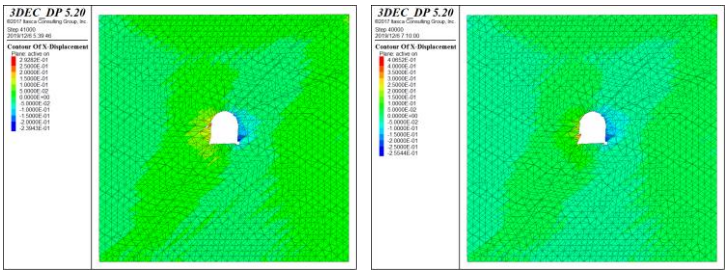

(d) 1800 m (e) 2000 m

Fig. 14 Horizontal deformation characteristics of the surrounding rock of jointed rock roadway under different buried depths

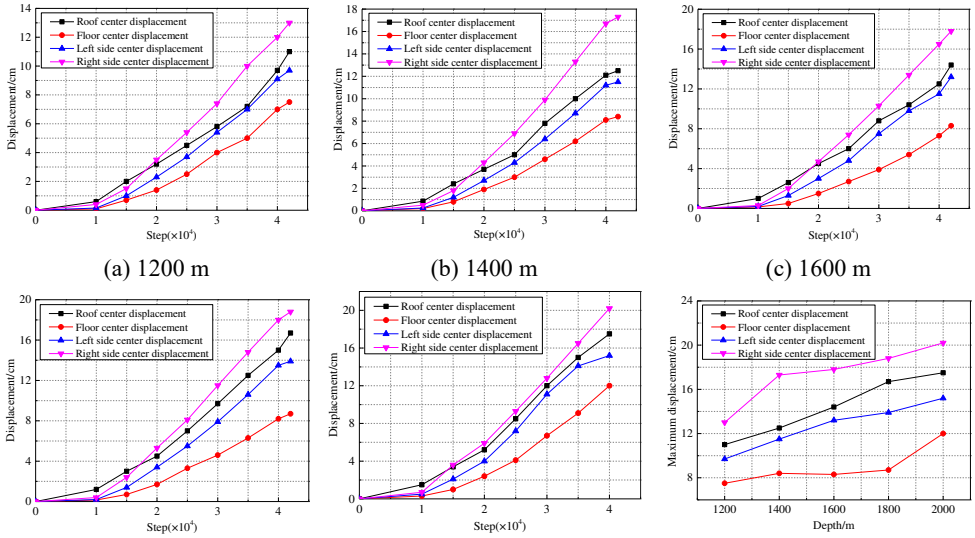

(a) 1200 m (b) 1400 m (c) 1600 m

(d) 1800 m (e) 2000 m (f) Maximum displacement

Fig. 15 Displacement at the center points of roof, floor, left side, and right side of the roadway under different burial depths

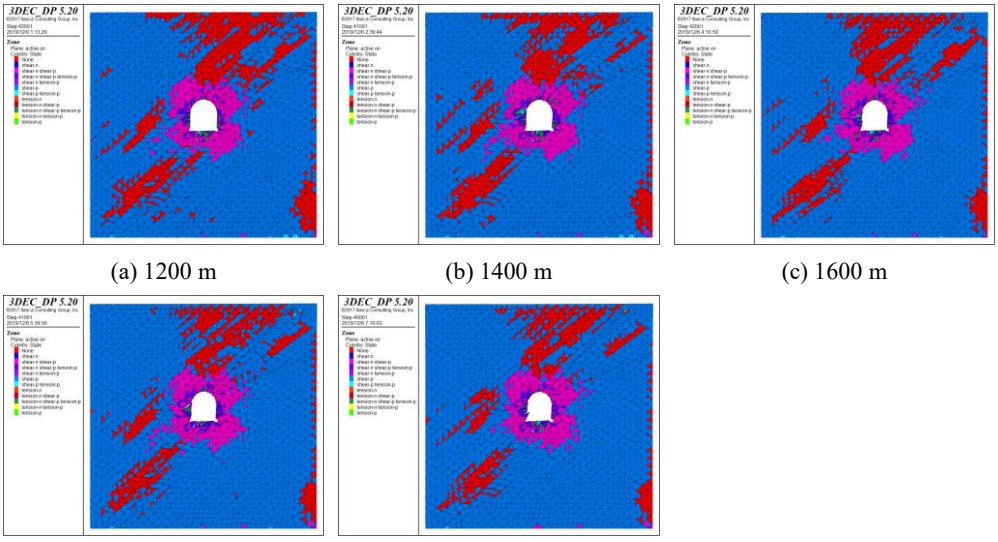

(a) 1200 m (b) 1400 m (c) 1600 m

(d) 1800 m (e) 2000 m

Fig. 16 Failure characteristics of the surrounding rock of jointed rock roadway under different buried depths

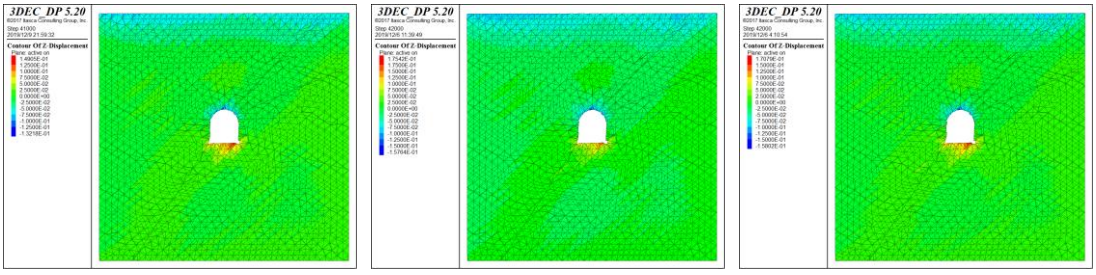

(a) 5 MPa (b) 10 MPa (c) 15.02 MPa

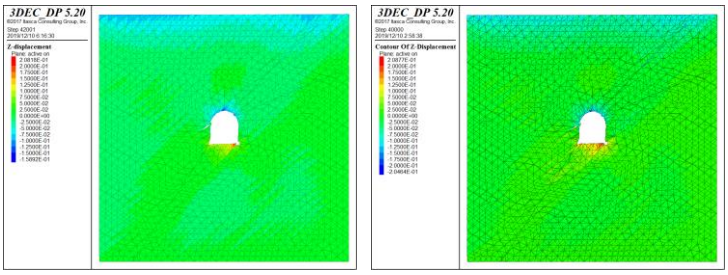

(d) 20 MPa (e) 25 MPa

Fig. 17 Vertical deformation characteristics of the surrounding rock of jointed rock roadway under different stress wave peaks

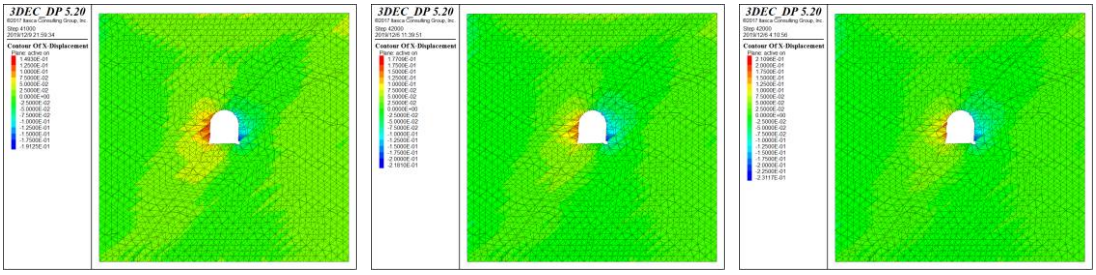

(a) 5 MPa (b) 10 MPa (c) 15.02 MPa

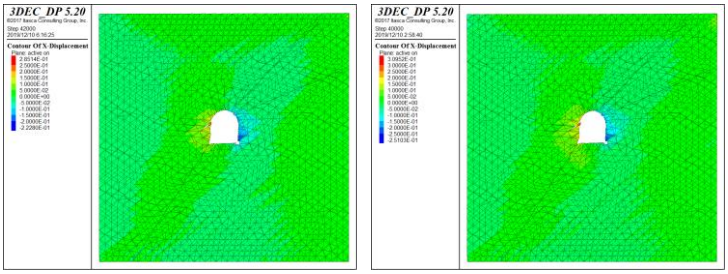

(d) 20 MPa (e) 25 MPa

Fig. 18 Horizontal deformation characteristics of the surrounding rock of jointed rock roadway under different stress wave peaks

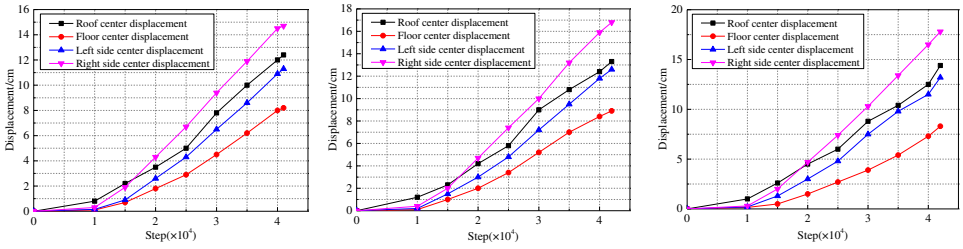

(a) 5 MPa (b) 10 MPa (c) 15.02 MPa

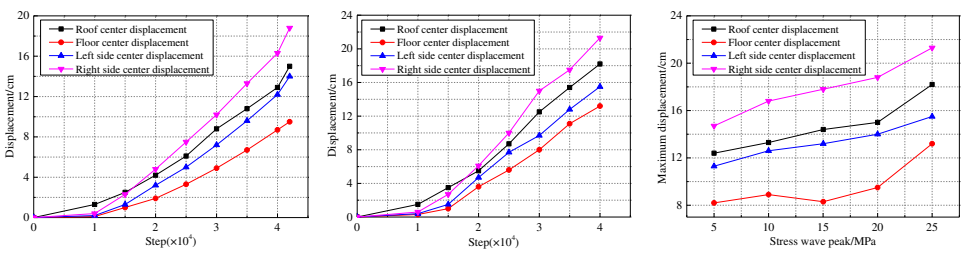

(d) 20 MPa (e) 25 MPa (f) Maximum displacement

Fig. 19 Displacement at the center points of roof, floor, left side, and right side of the roadway under different stress wave peaks

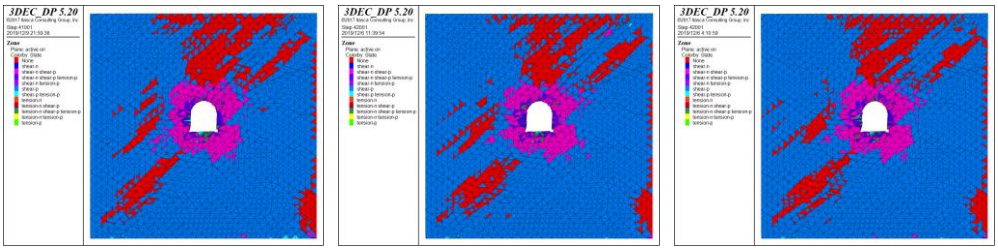

(a) 5 MPa (b) 10 MPa (c) 15.02 MPa

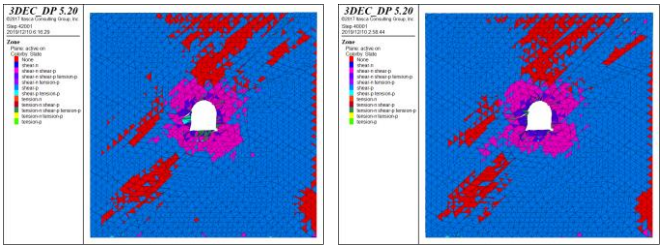

(d) 20 MPa (e) 25 MPa

Fig. 20 Failure characteristics of the surrounding rock of jointed rock roadway under different stress wave peaks

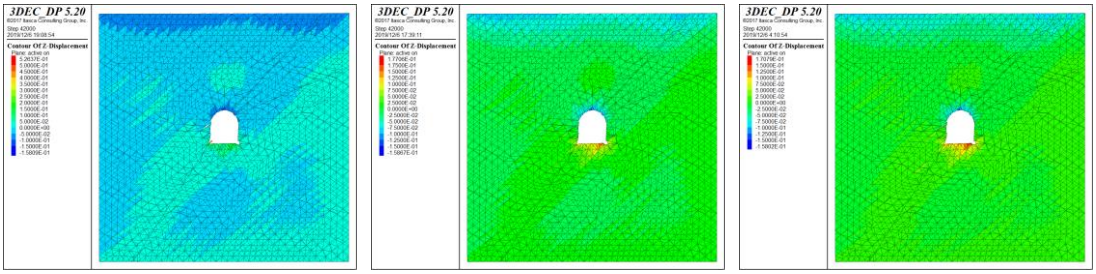

(a) 40 Hz (b) 30 Hz (c) 20 Hz

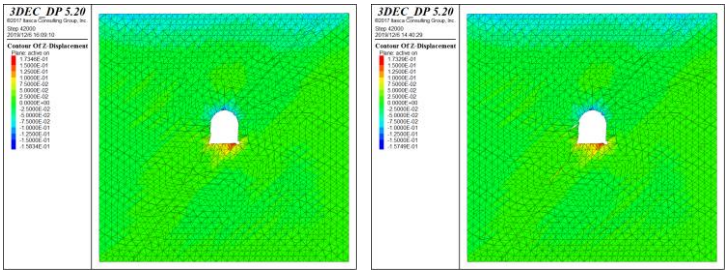

(d) 10 Hz (e) 5 Hz

Fig. 21 Vertical deformation characteristics of the surrounding rock of jointed rock roadway under different stress wave delays

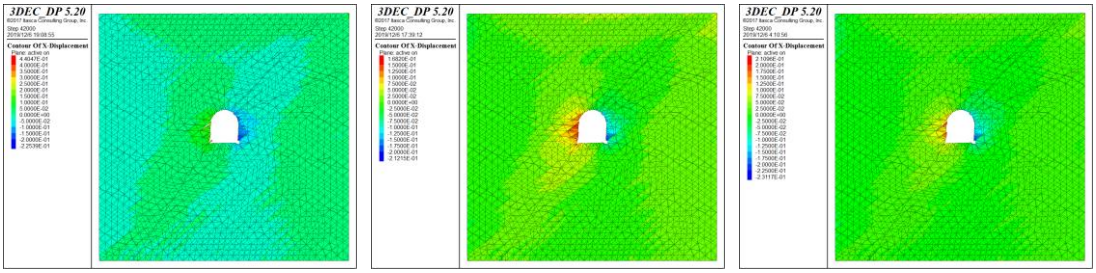

(a) 40 Hz (b) 30 Hz (c) 20 Hz

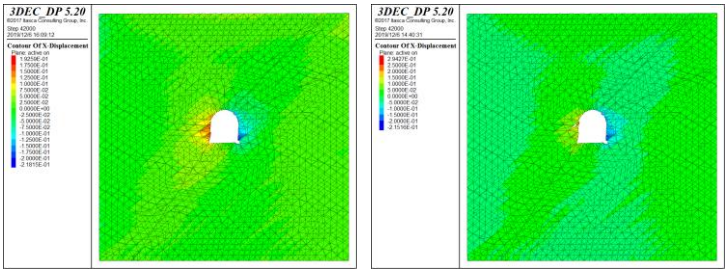

(d) 10 Hz (e) 5 Hz

Fig. 22 Horizontal deformation characteristics of the surrounding rock of jointed rock roadway under different stress wave delays

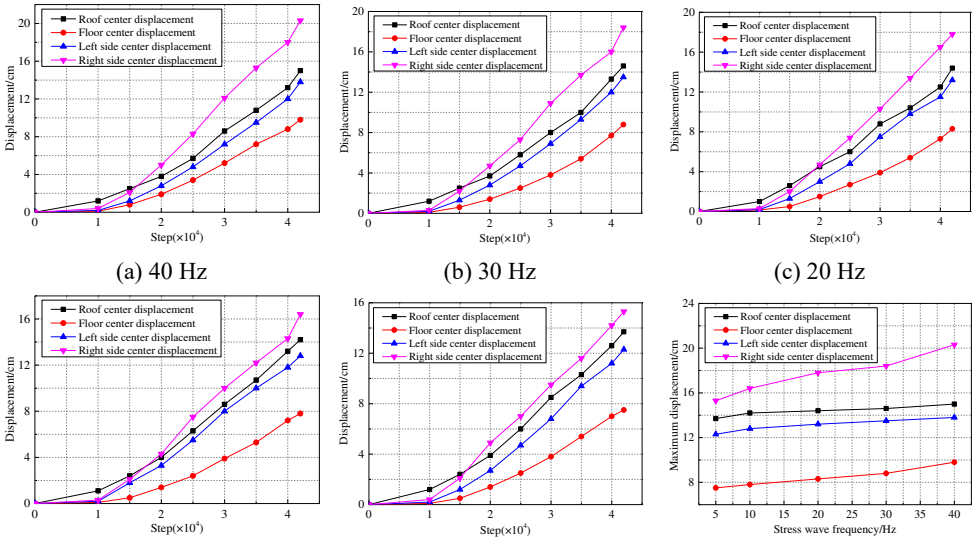

(a) 40 Hz (b) 30 Hz (c) 20 Hz

(d) 10 Hz (e) 5 Hz (f) Maximum displacement

Fig. 23 Displacement at the center points of roof, floor, left side, and right side of the roadway under different stress wave delays

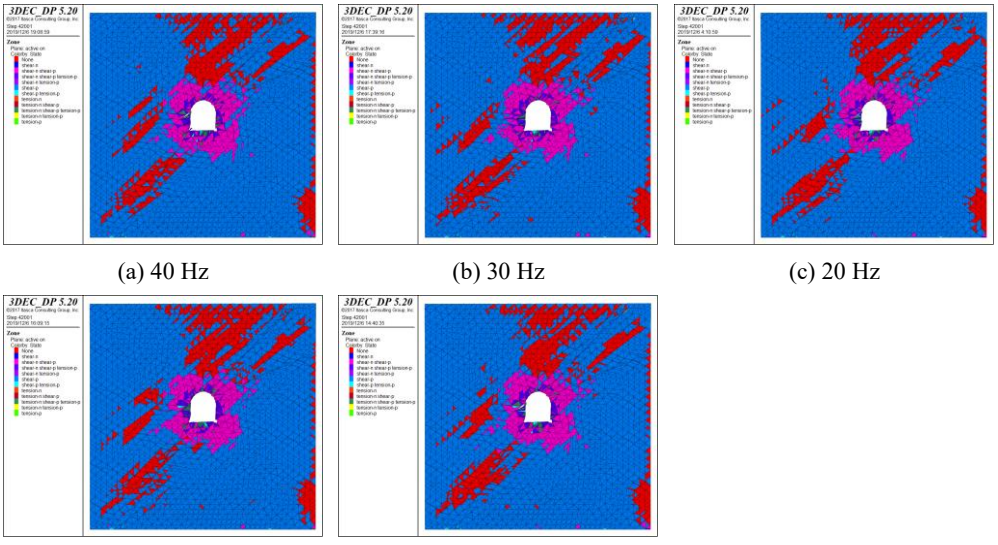

(a) 40 Hz (b) 30 Hz (c) 20 Hz

(d) 10 Hz (e) 5 Hz

Fig. 24 Failure characteristics of the surrounding rock of jointed rock roadway under different stress wave delays

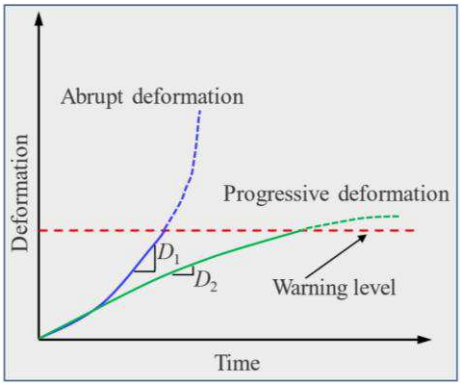

Fig. 25 Convergence curve of roadway with gradual and abrupt deformation (after Sagong et al. (2011))

TABLES

Table 1

In-situ stress measurement results in the gold mine.

No.	Depth (m)	The maximum principal stress (σ_1)			The intermediate principal stress (σ_2)			The minimum principal stress (σ_3)		
		Value (MPa)	Direction (deg)	Dip angle (deg)	Value (MPa)	Direction (deg)	Dip angle (deg)	Value (MPa)	Direction (deg)	Dip angle (deg)
1	75	6.01	288.5	-6.3	3.81	198.0	-4.9	2.56	250.4	82.0
2	150	7.73	280.9	-5.2	5.48	9.4	16.6	4.50	27.7	72.5
3	420	19.27	284.1	-21.3	11.05	18.5	-11.1	10.88	134.4	-65.7
4	420	19.69	120.4	-14.9	10.92	169.2	68.1	9.44	34.7	15.8
5	510	24.55	129	4	16.35	-138	2	14.49	133	-85
6	510	24.64	-111	3	15.68	155	82	15.02	161	-10
7	555	25.71	-45	-13	14.00	14	73	13.00	50	-20
8	600	28.88	103	1	16.54	10	76	14.77	13	-8
9	600	30.17	110	-16	18.83	24	-11	16.94	236	-70
10	645	29.57	112	-3	19.56	-177	-80	15.48	-156	-9
11	690	31.50	-80	2	19.08	230	-79	17.54	10	-10
12	690	29.77	-83	4	20.84	-8	-74	19.63	8	15
13	750	33.22	119	-10	19.93	-89	-82	17.10	208	-8
14	750	32.78	105.6	-0.59	19.6	18.7	79.2	16.68	15.5	-10.8
15	780	30.72	133.3	-14.9	26.41	-135.6	-4.17	18.09	149.7	74.5

Table 2

Mechanical parameters of the rock mass.

Density /(kg/m^3)	Bulk modulus /GPa	Shear modulus /GPa	Tensile strength /MPa	Cohesion /MPa	Internal friction angle /°
2629	9.89	7.34	5.18	8.73	30.59

Table 3

Mechanical parameters of the joints.

Normal stiffness /GPa·m^{-1}	Tangential stiffness /GPa·m^{-1}	Tensile strength /MPa	Cohesion /MPa	Internal friction angle /°
25.81	18.27	0.55	2.41	35.16

Figures

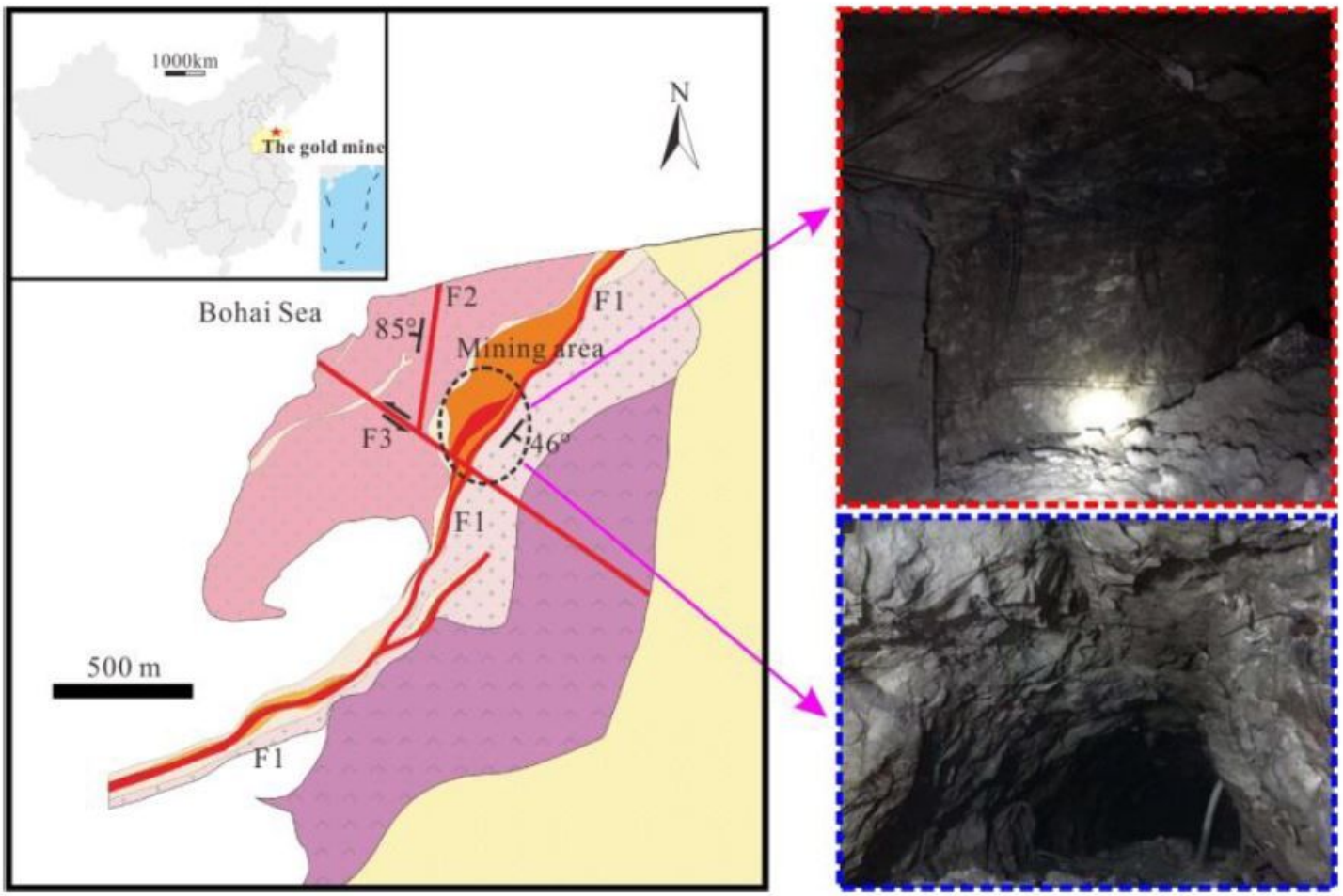

Figure 1

The geographical location of the gold mine and typical roadway deformation in the local area

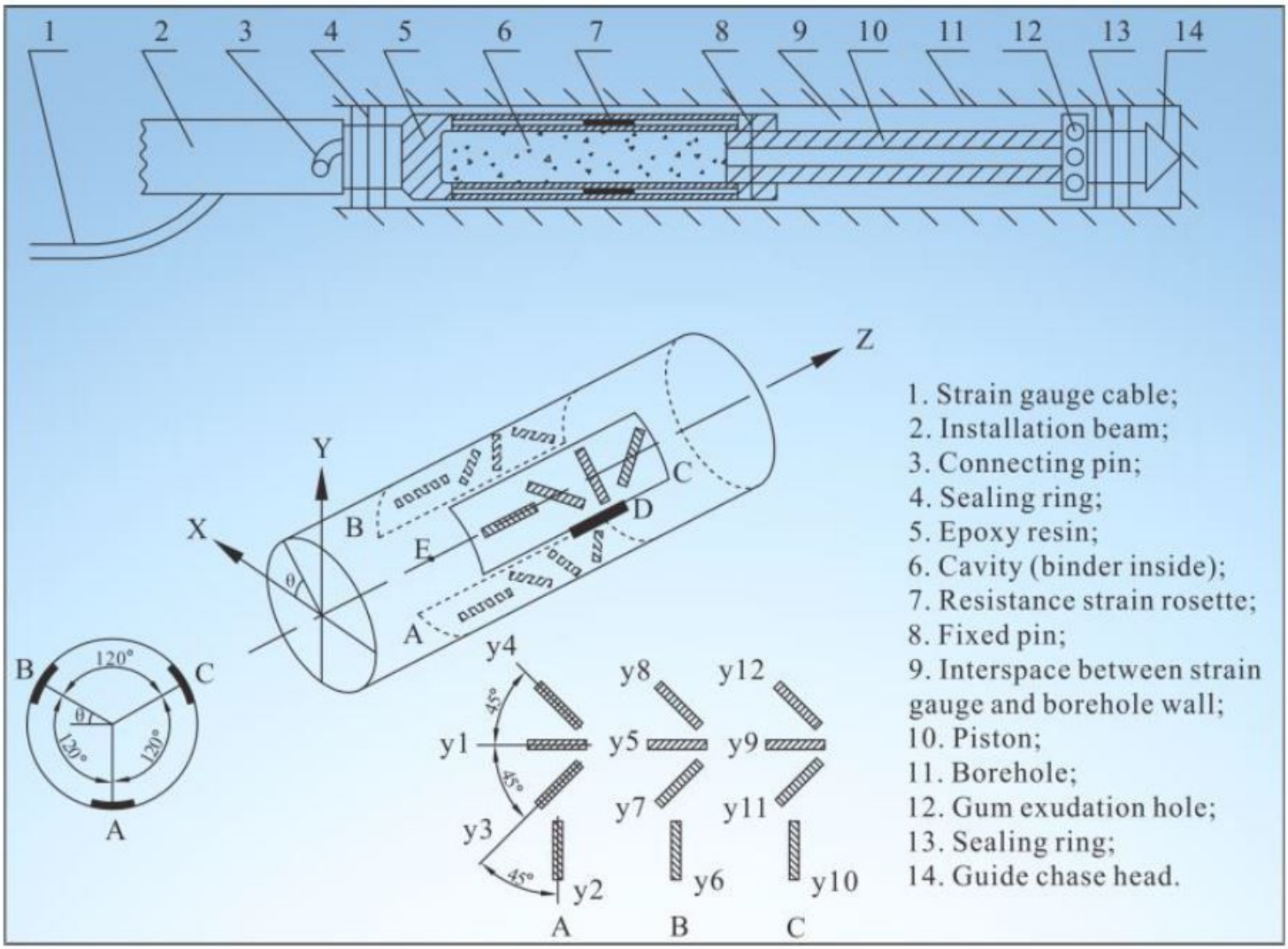

Figure 2

Schematic diagram of hollow inclusion strain gauge with complete temperature compensation

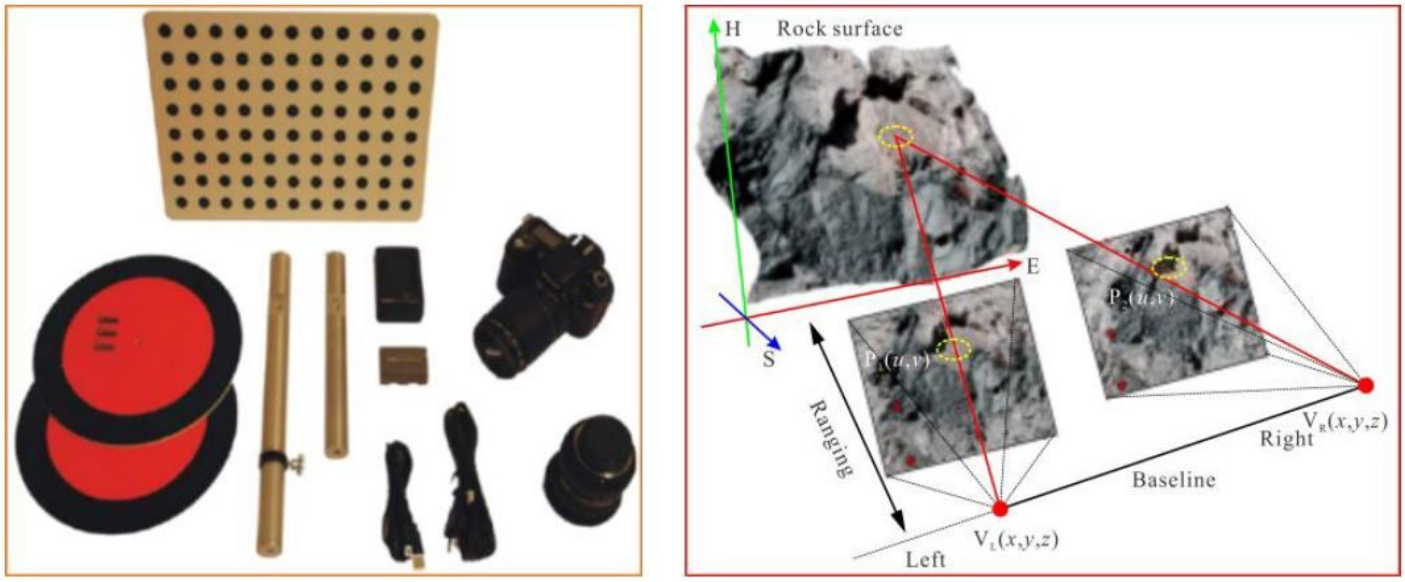

Figure 3

Shapemetrix 3D measurement system (a) and the measuring principle of the system (b)

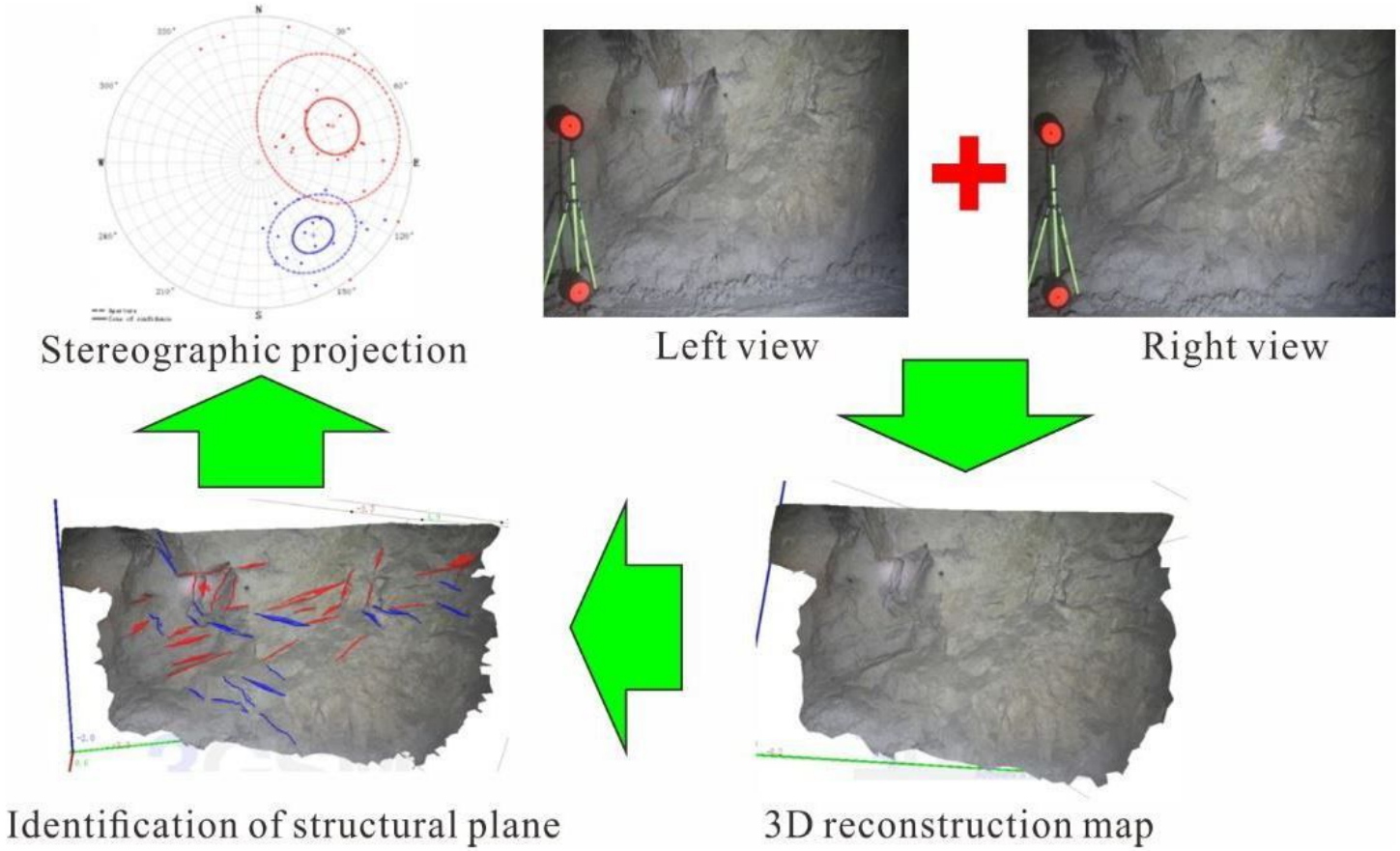

Figure 4

Illustration of information collection for structural planes of surrounding rock of the roadway

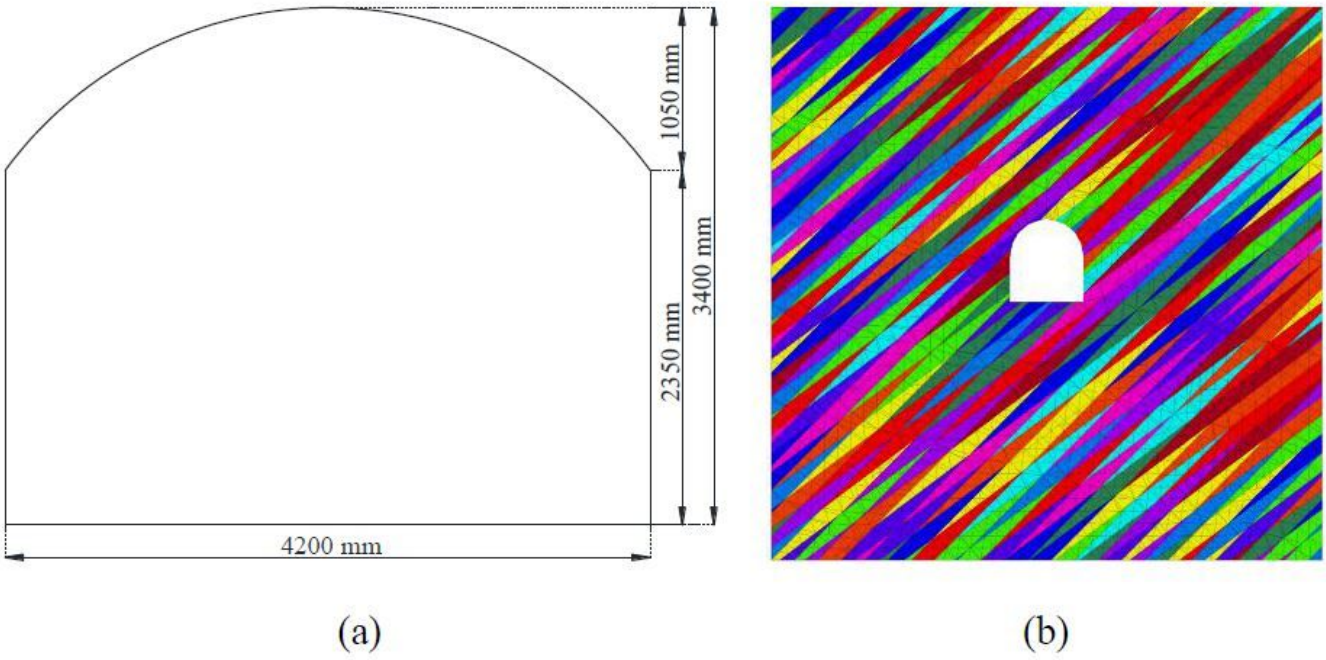

Figure 5

Roadway size (a) and plane display of calculation model of jointed rock roadway (b)

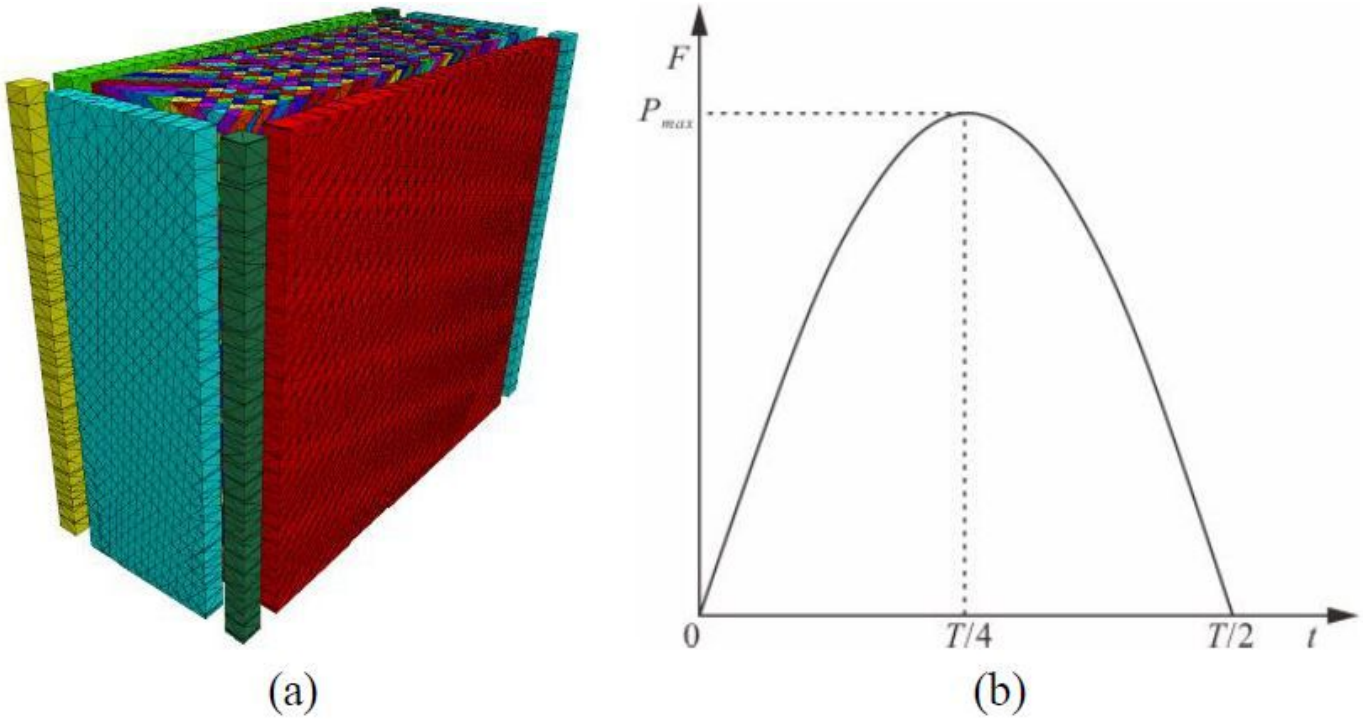

Figure 6

Free field boundary (a) and stress wave time history curve (b)

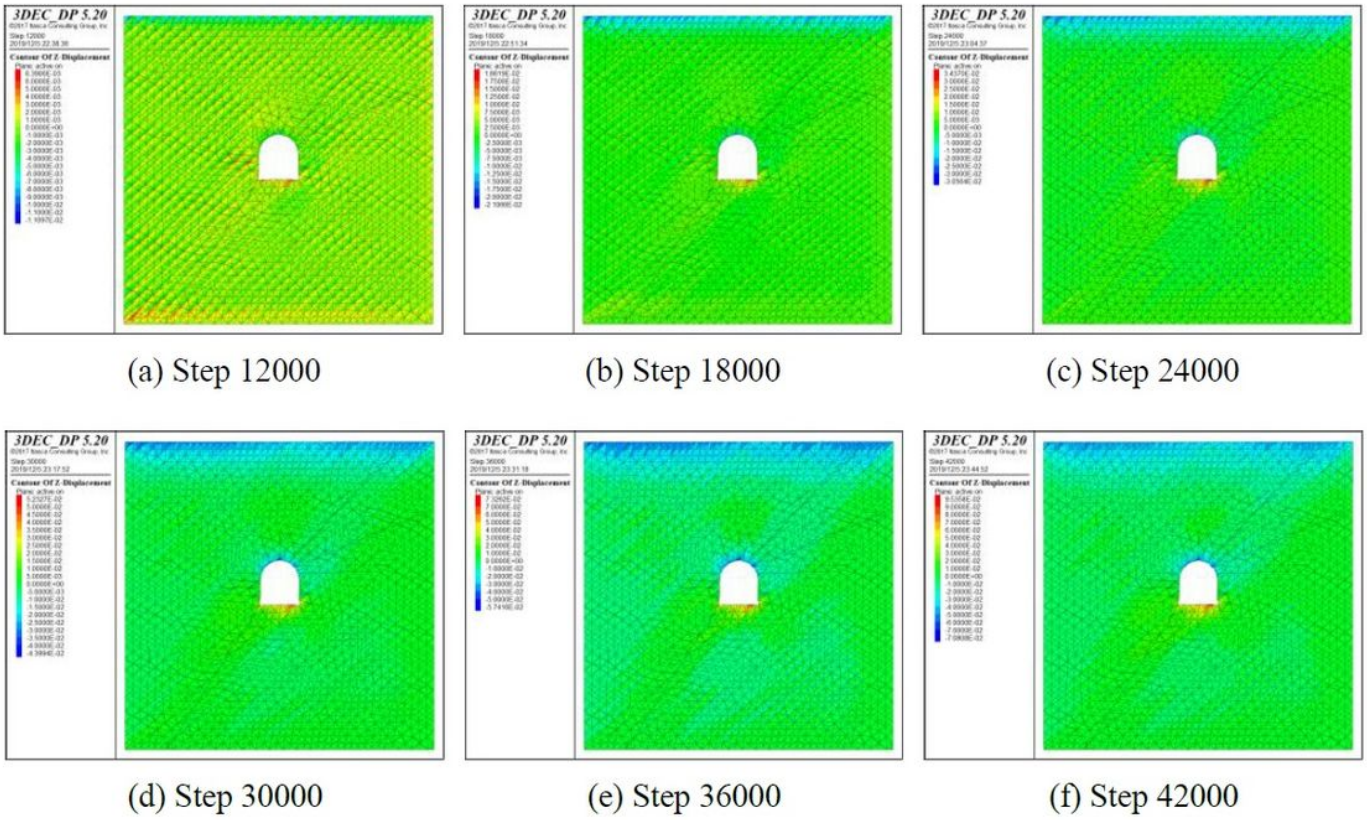

Figure 7

Vertical displacement evolution contours of the surrounding rock in the jointed rock roadway

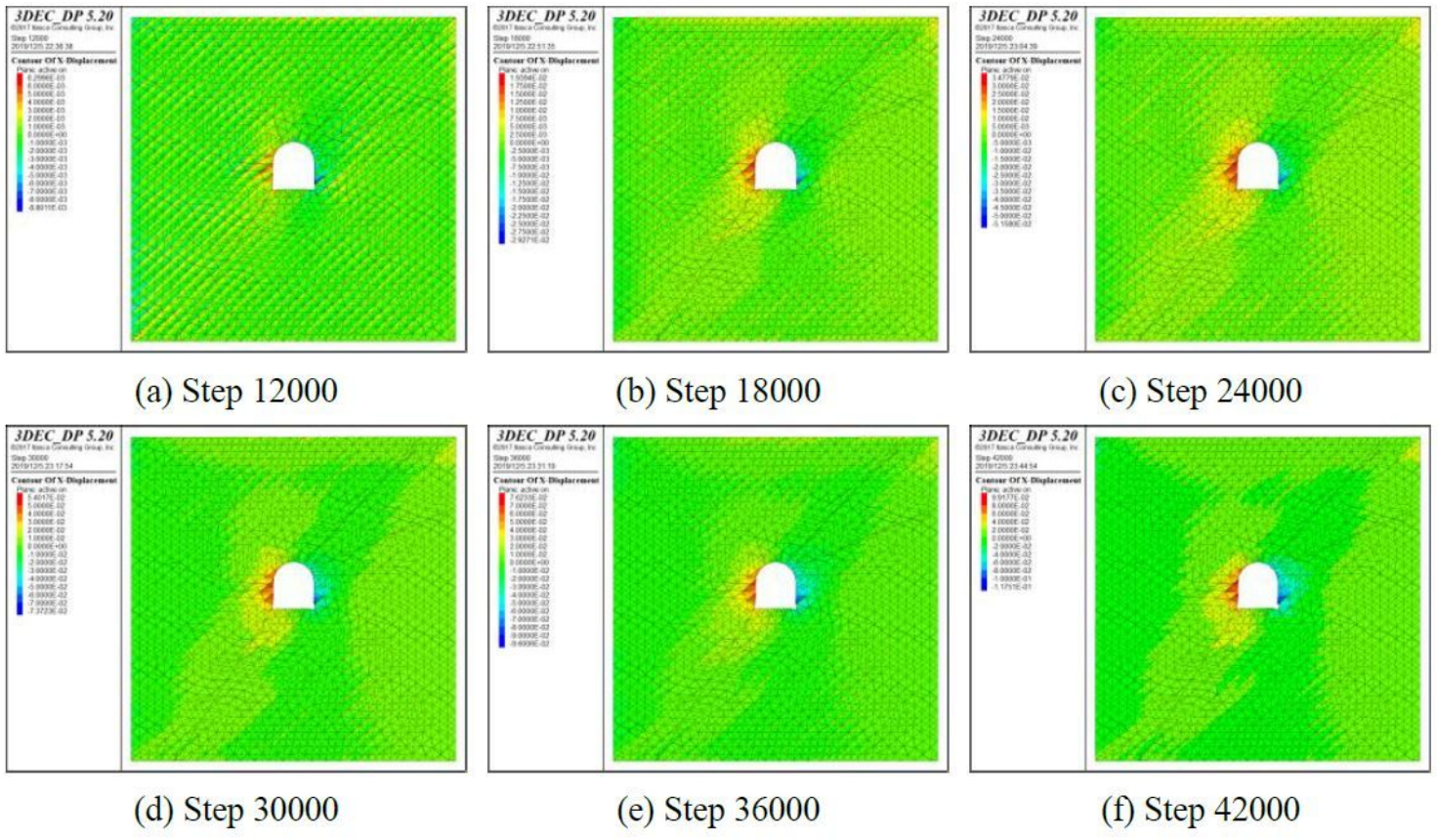

Figure 8

Horizontal displacement evolution contours of the surrounding rock in the jointed rock roadway

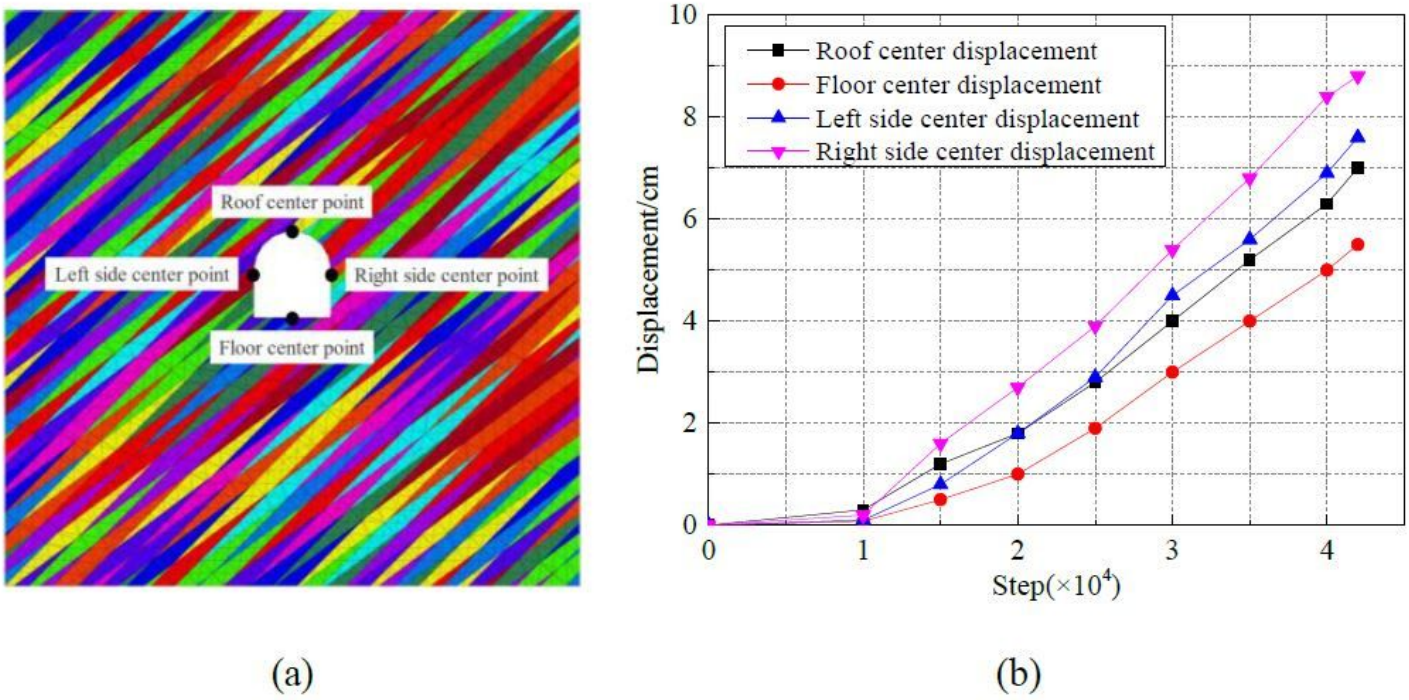

Figure 9

Location of monitoring points (a) and displacement of center points of roof, floor, left side, and right side of the roadway (b)

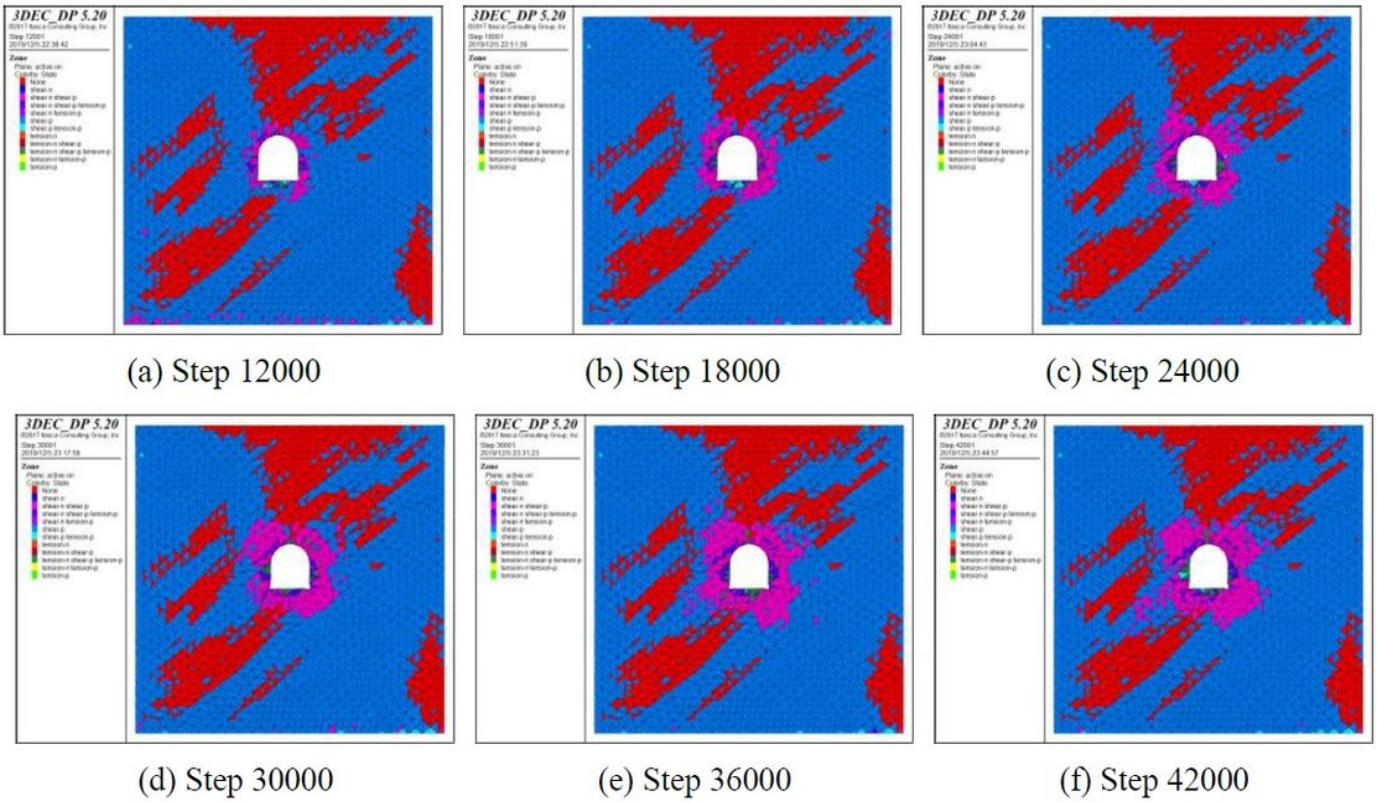

Figure 10

Evolution contours of the plastic zone of the surrounding rock of jointed rock roadway

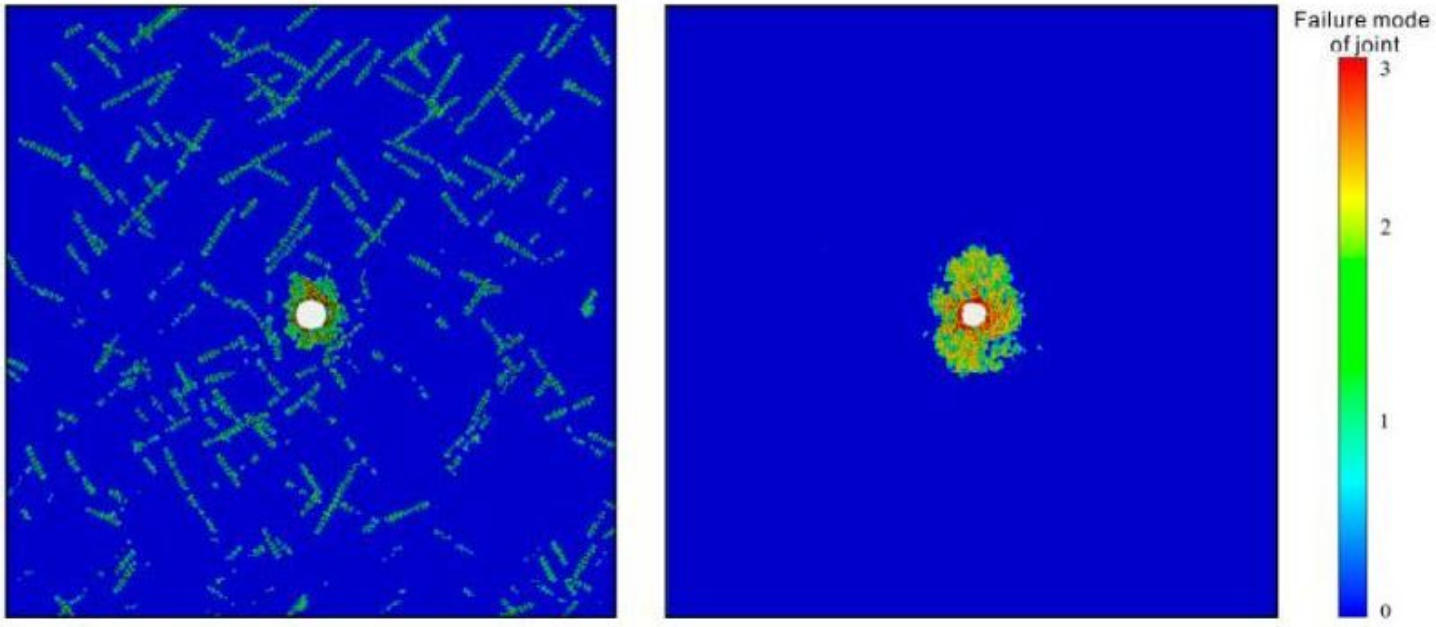

Figure 11

Failure modes of surrounding rock of random jointed circular roadway (Liu et al. 2019)

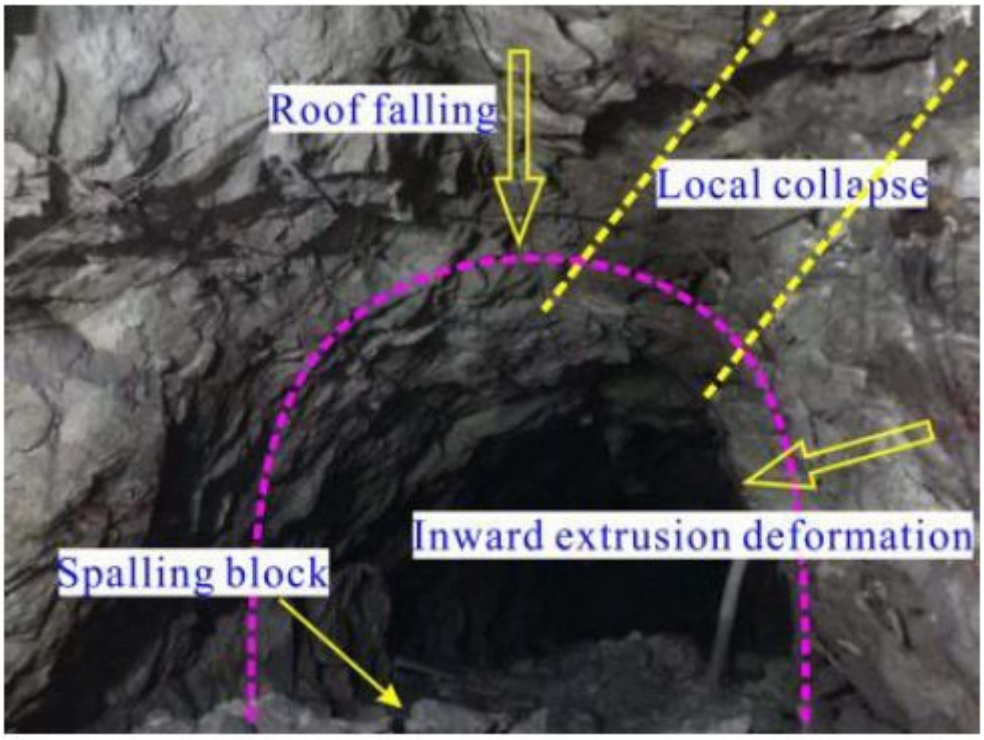

Figure 12

Deformation and failure of roadway surrounding rock in the engineering field (

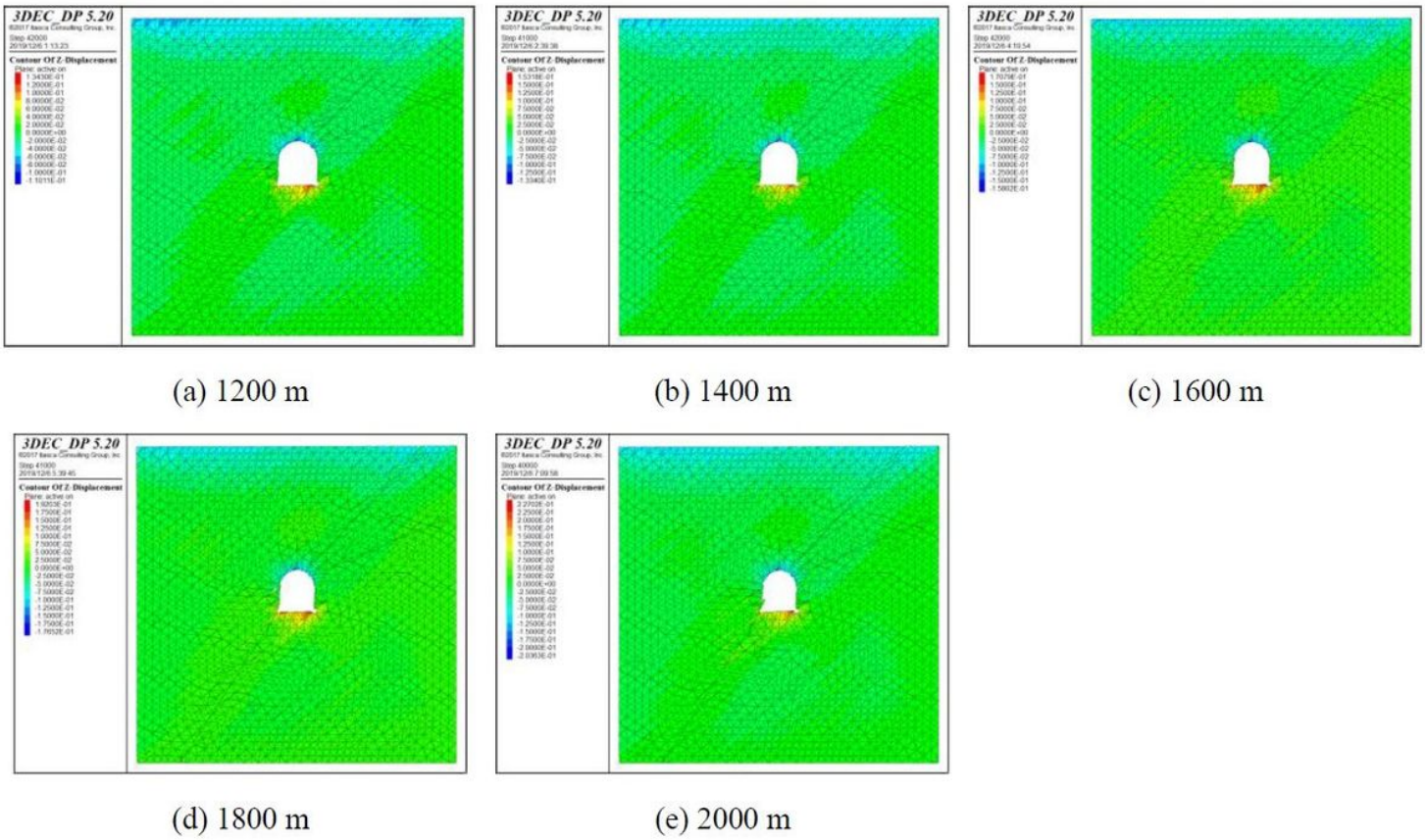

Figure 13

Vertical deformation characteristics of the surrounding rock of jointed rock roadway under different buried depths

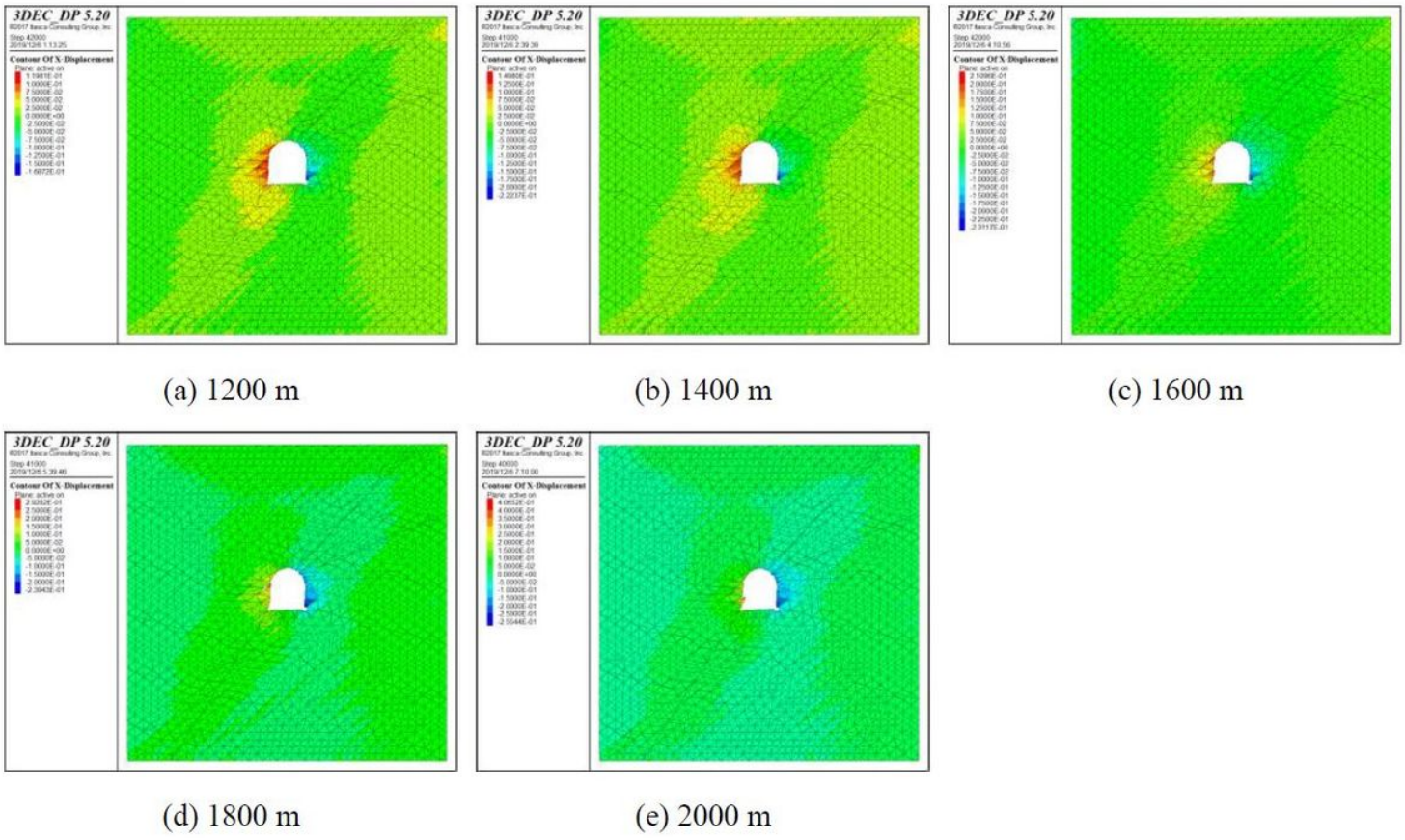

Figure 14

Horizontal deformation characteristics of the surrounding rock of jointed rock roadway under different buried depths

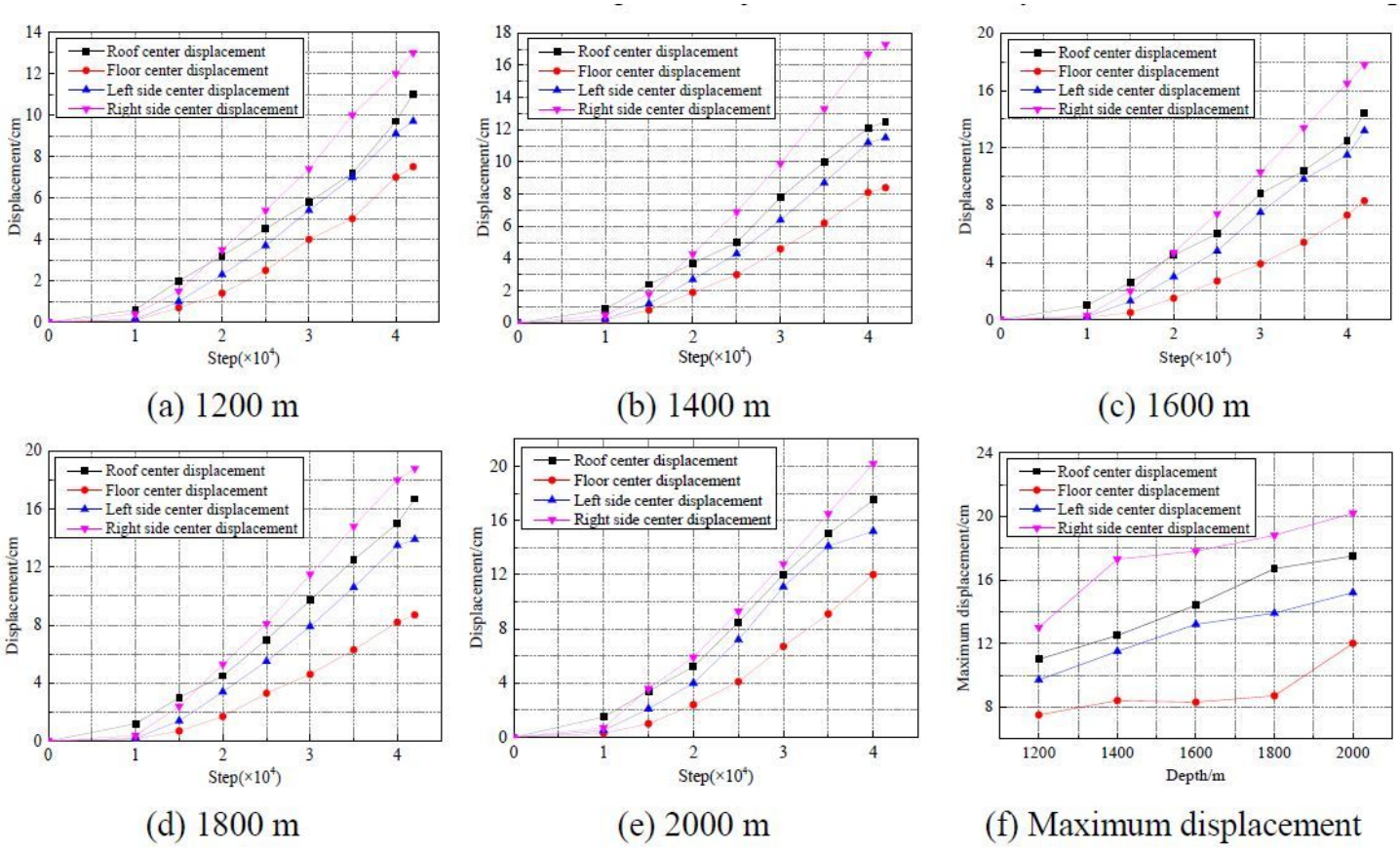

Figure 15

Displacement at the center points of roof, floor, left side, and right side of the roadway under different burial depths

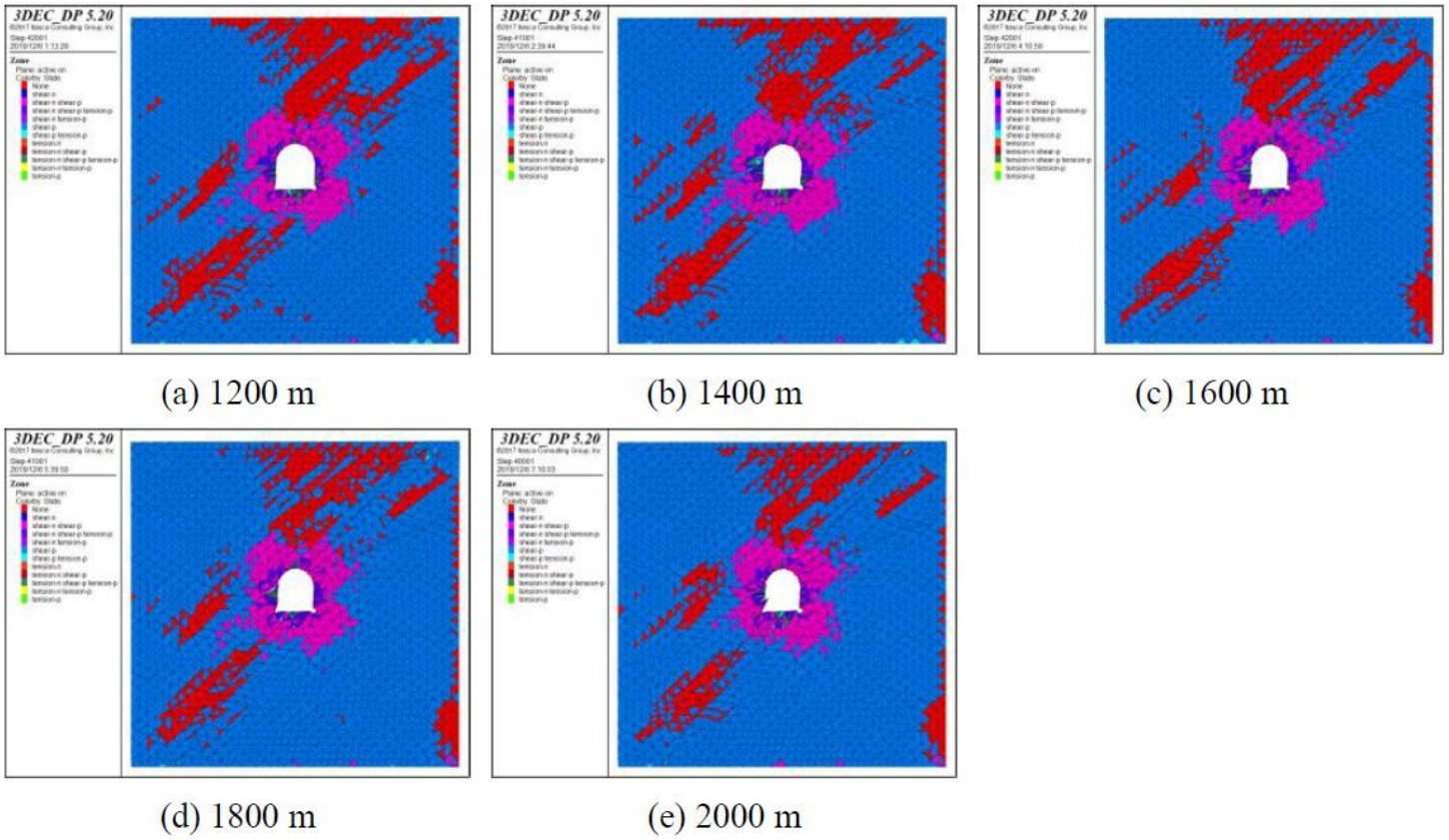

Figure 16

Failure characteristics of the surrounding rock of jointed rock roadway under different buried depths

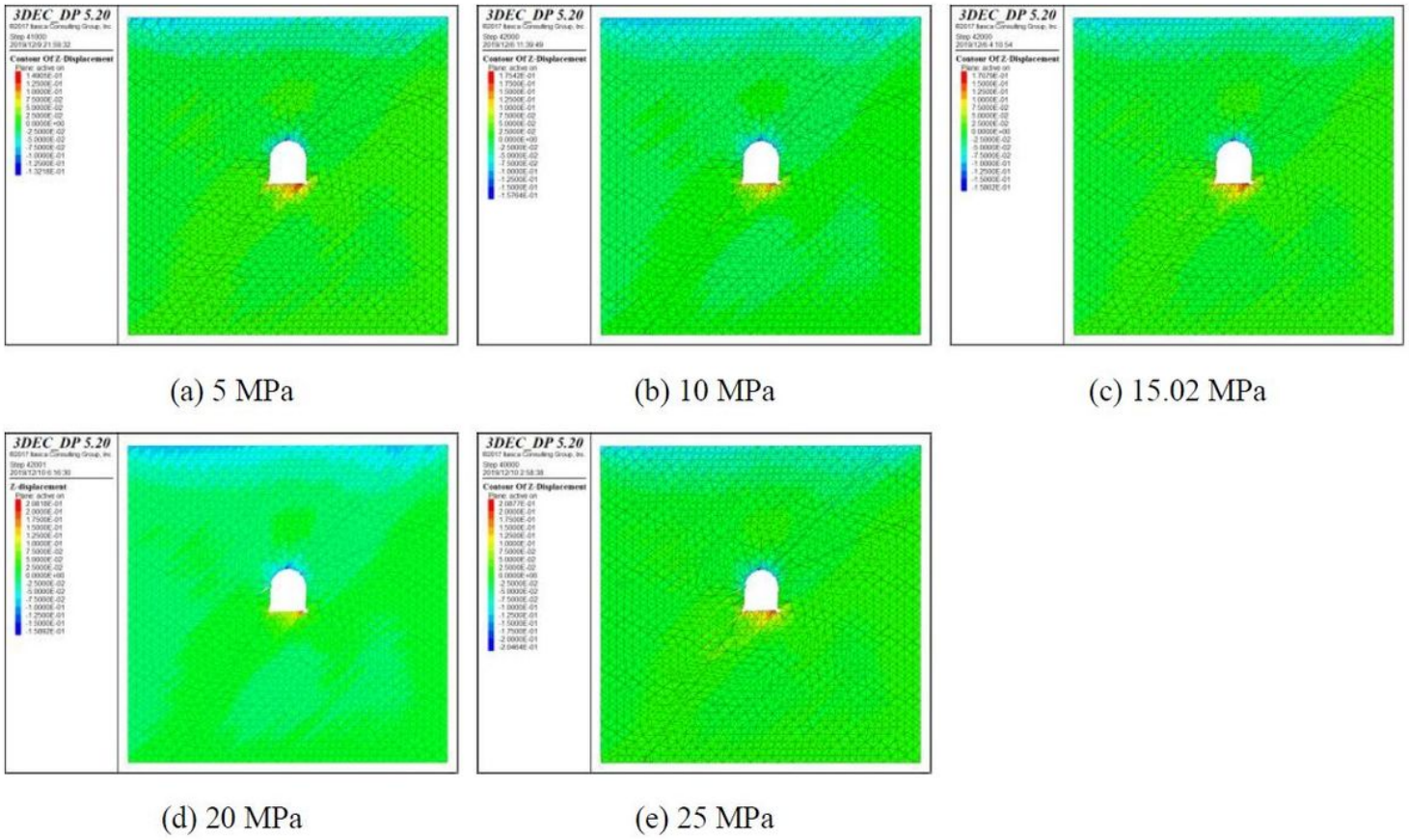

Figure 17

Vertical deformation characteristics of the surrounding rock of jointed rock roadway under different stress wave peaks

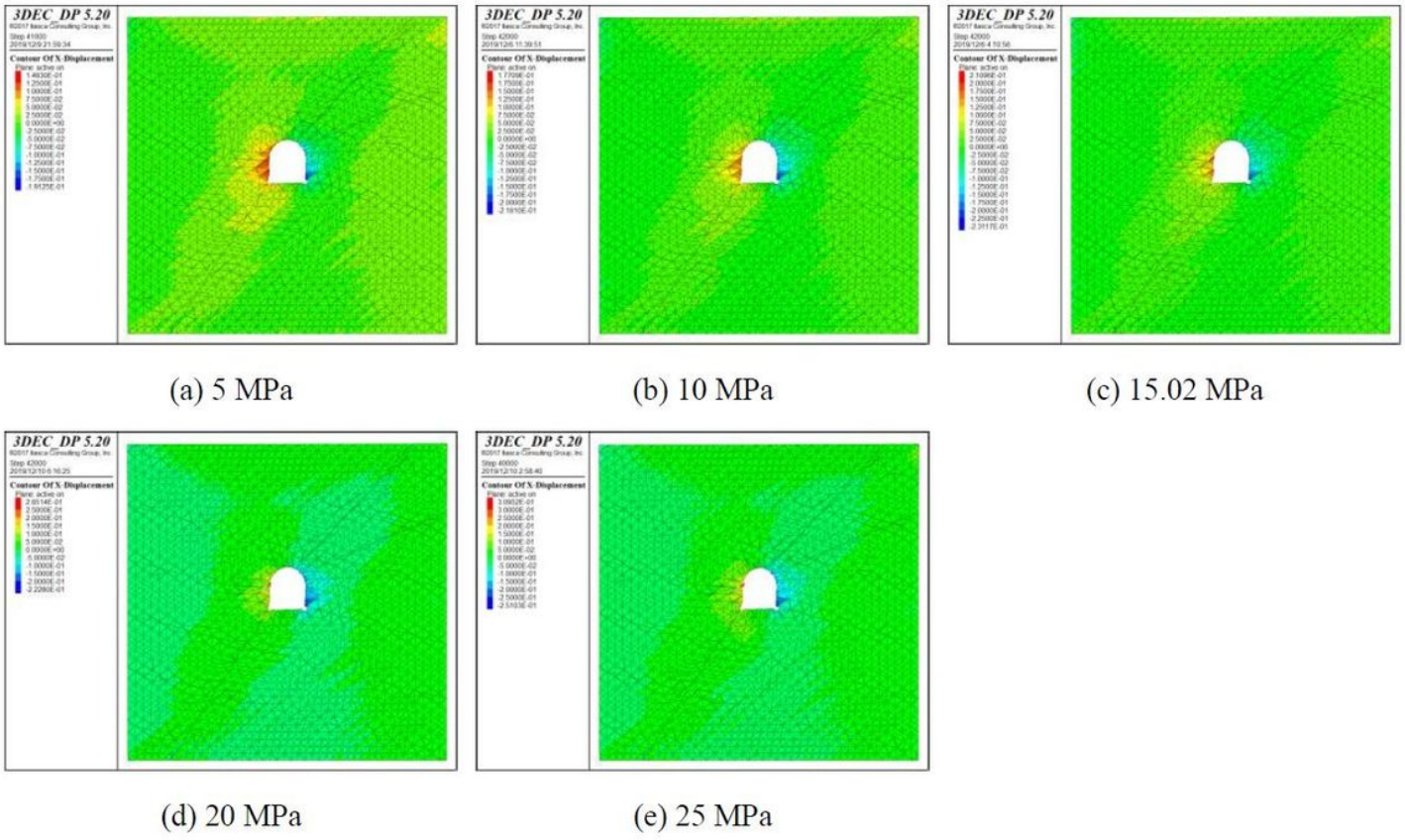

Figure 18

Horizontal deformation characteristics of the surrounding rock of jointed rock roadway under different stress wave peaks

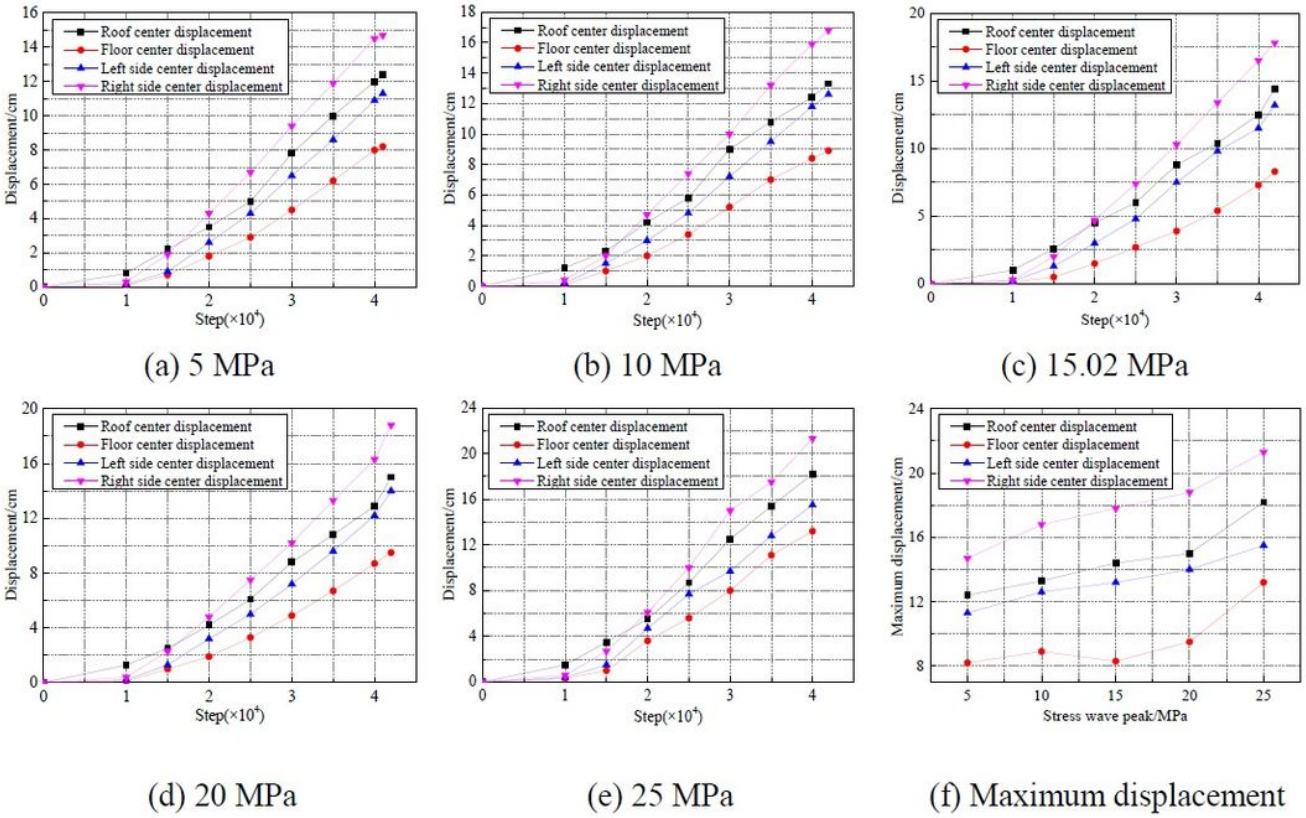

Figure 19

Displacement at the center points of roof, floor, left side, and right side of the roadway under different stress wave peaks

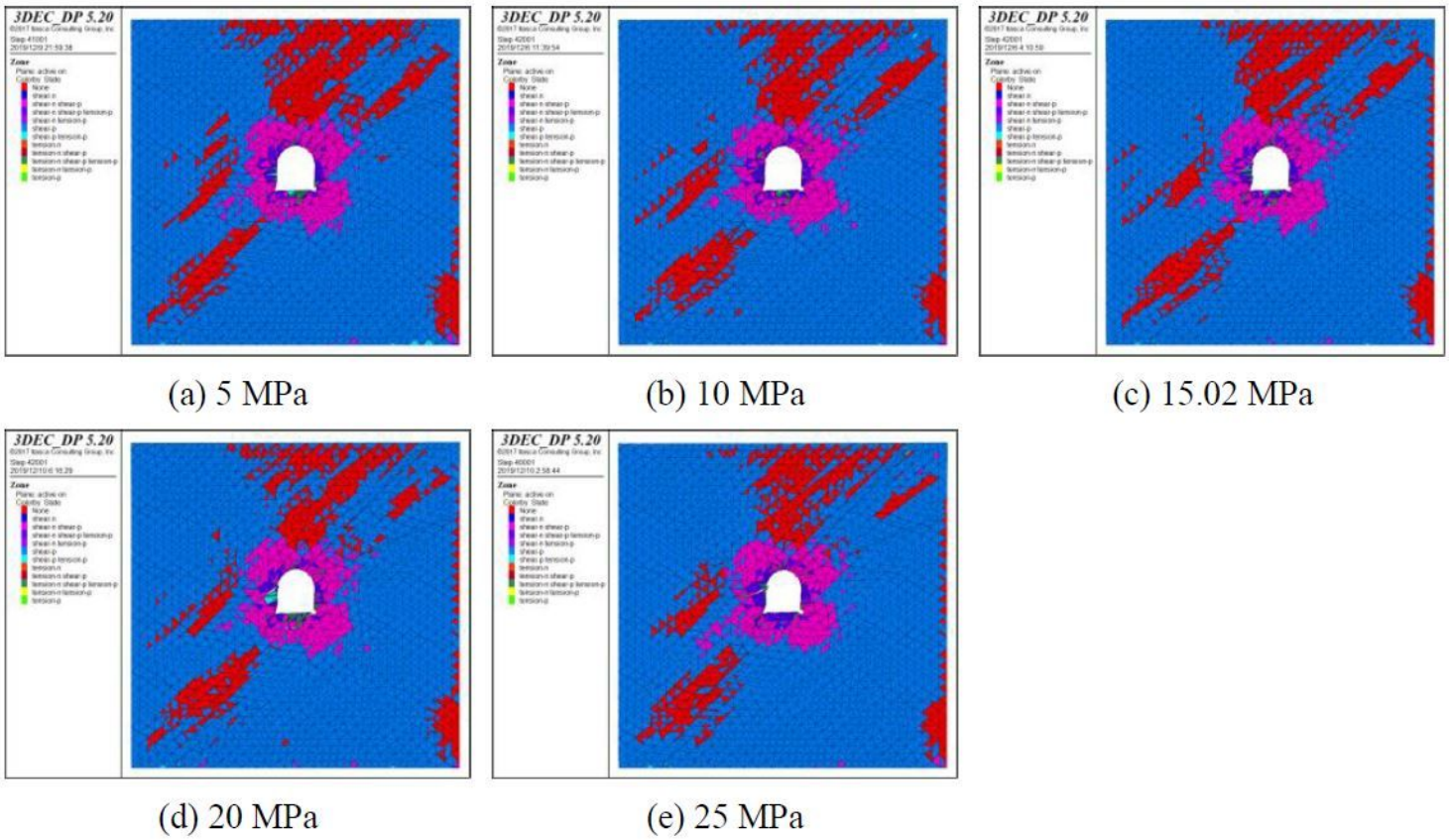

Figure 20

Failure characteristics of the surrounding rock of jointed rock roadway under different stress wave peaks

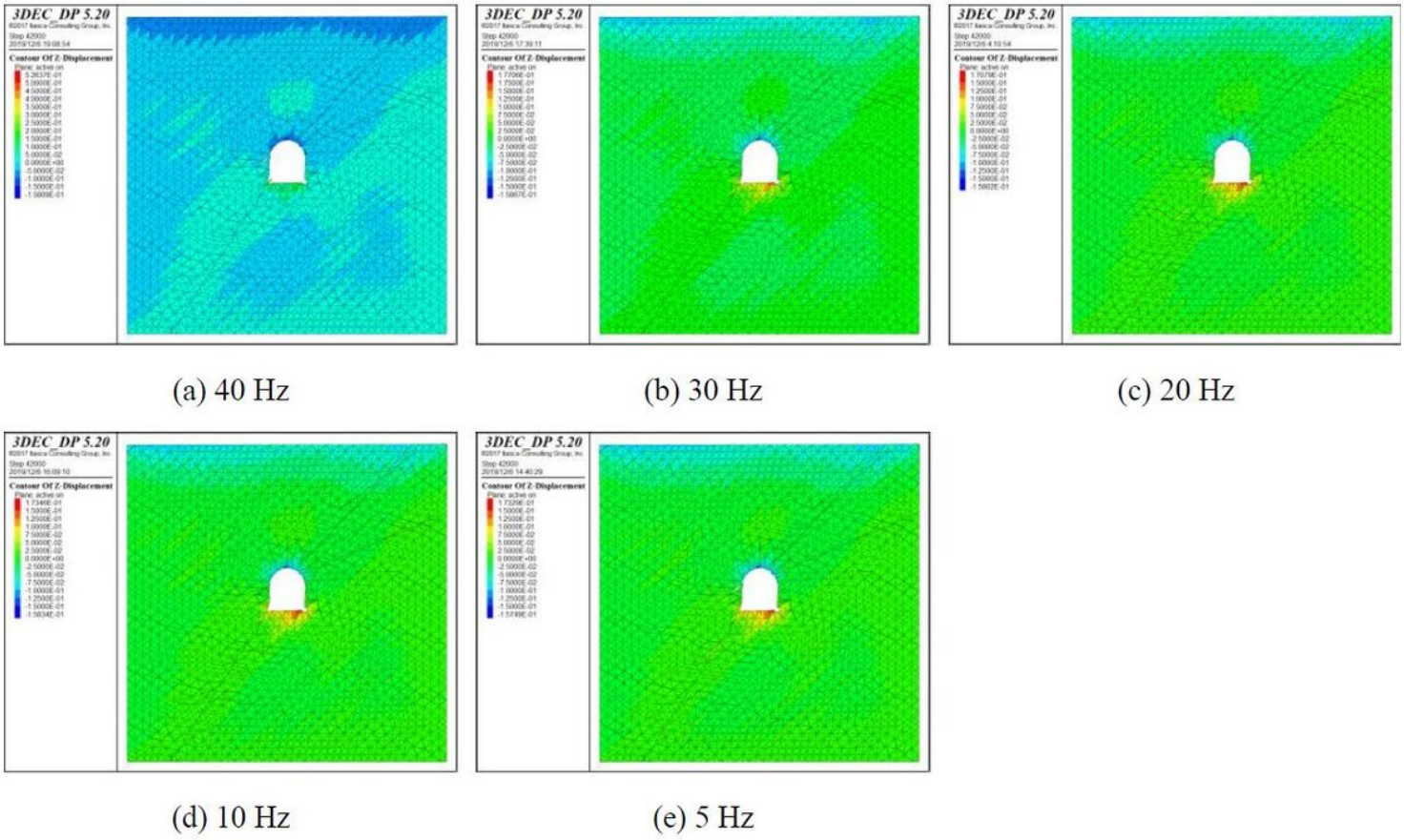

Figure 21

Vertical deformation characteristics of the surrounding rock of jointed rock roadway under different stress wave delays

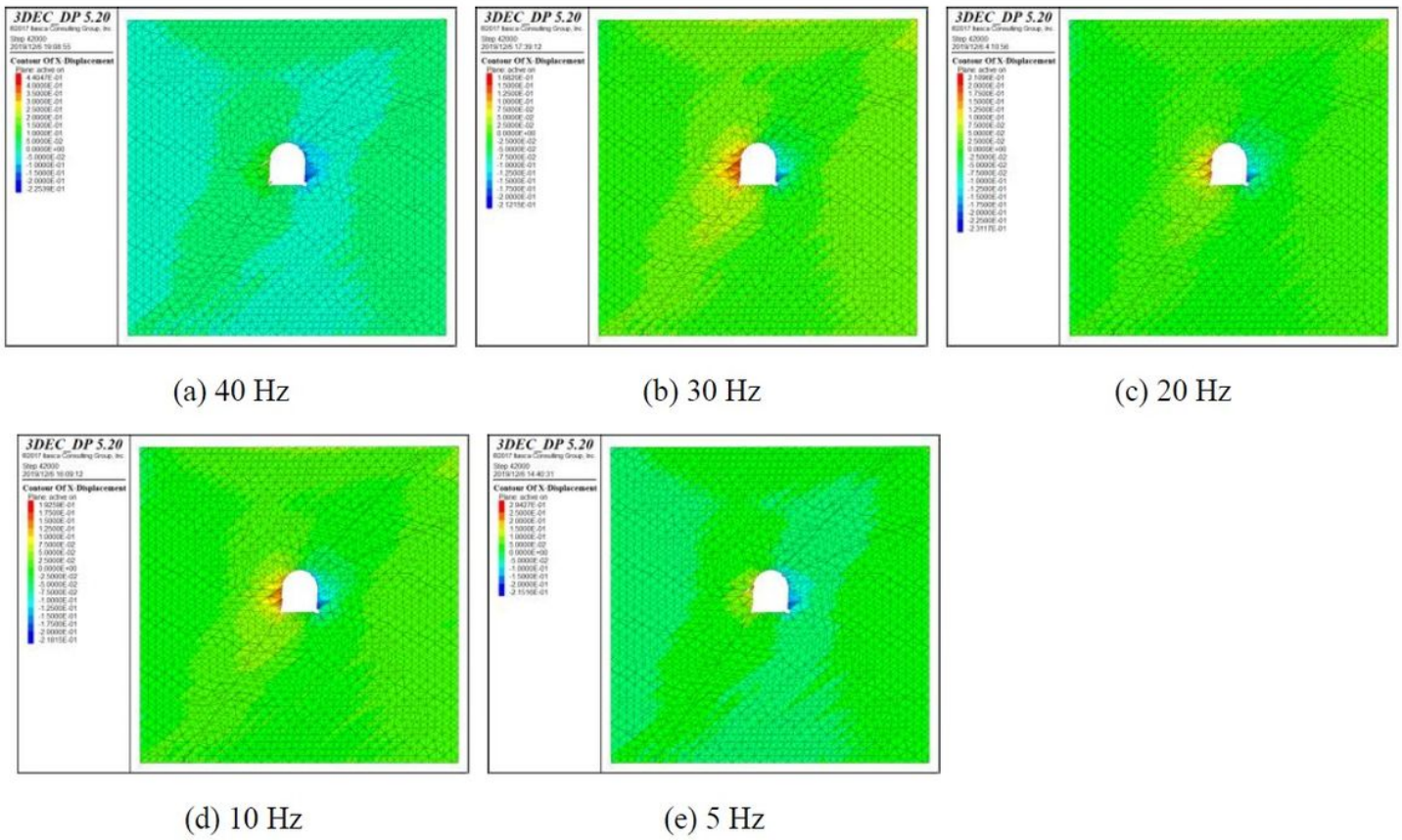

Figure 22

Horizontal deformation characteristics of the surrounding rock of jointed rock roadway under different stress wave delays

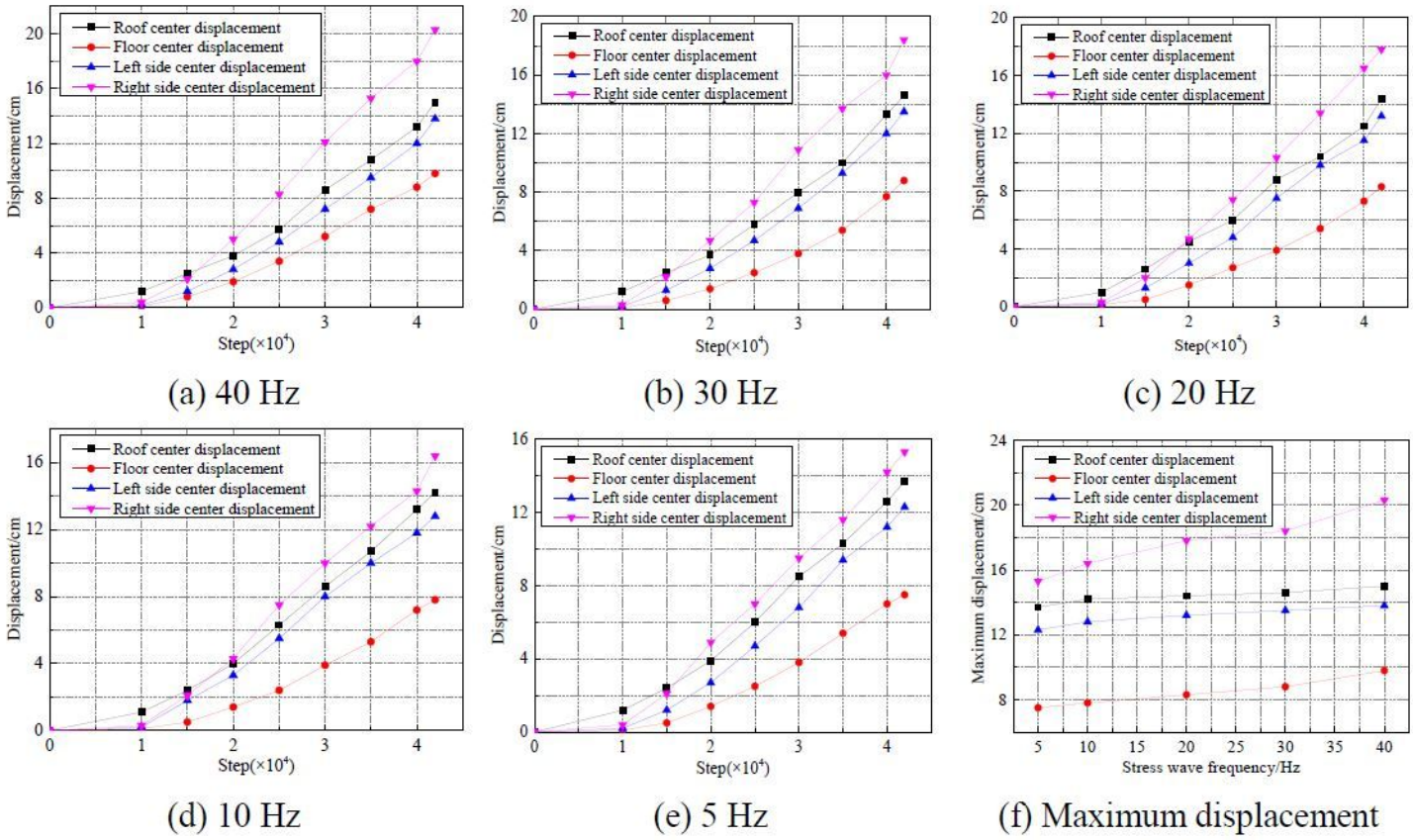

Figure 23

Displacement at the center points of roof, floor, left side, and right side of the roadway under different stress wave delays

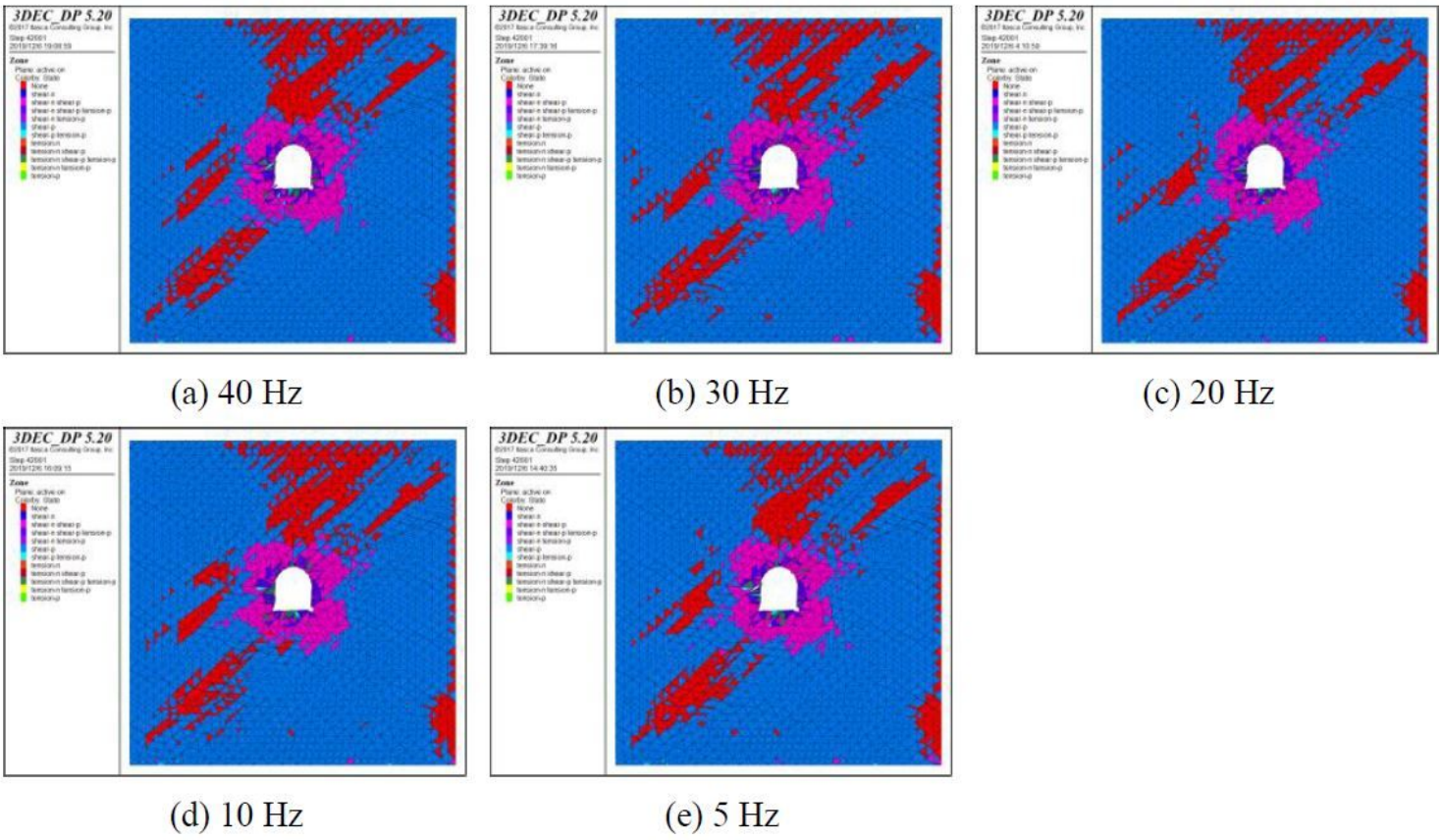

Figure 24

Failure characteristics of the surrounding rock of jointed rock roadway under different stress wave delays

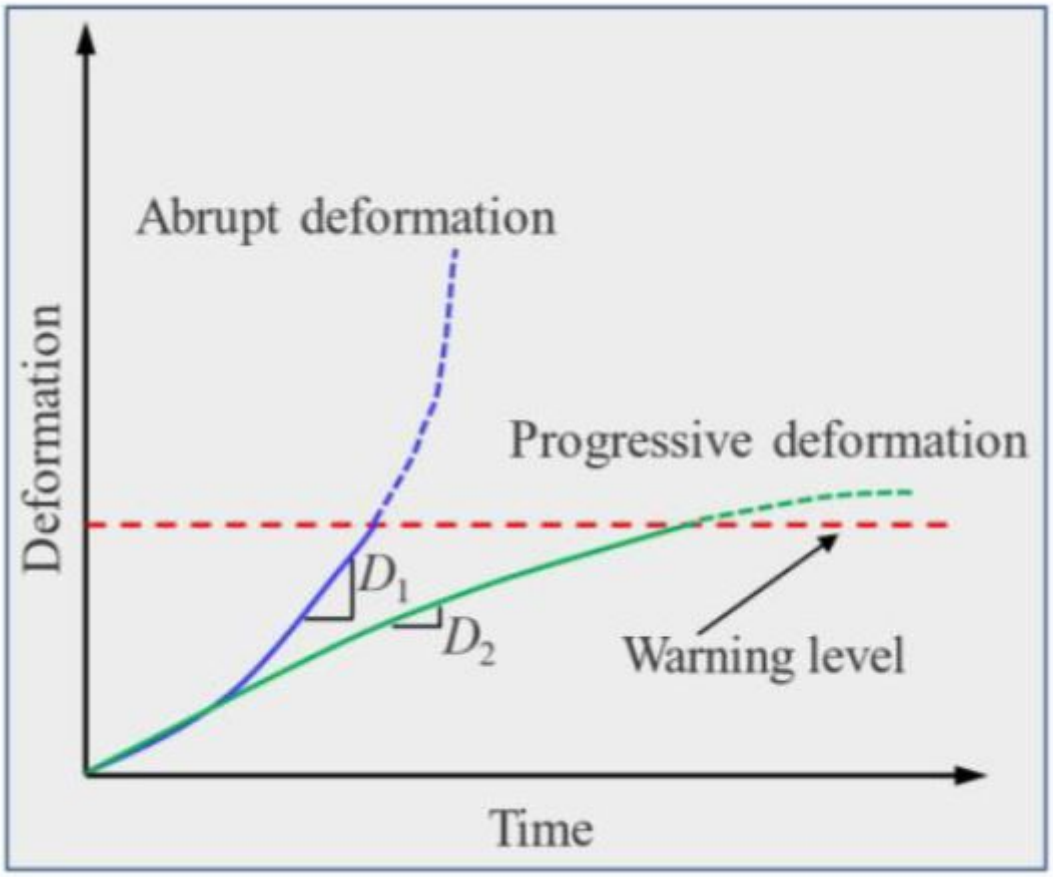

Figure 25

Convergence curve of roadway with gradual and abrupt deformation (after Sagong et al. (2011))